

**T.C.
YILDIZ TECHNICAL UNIVERSITY
GRADUATE SCHOOL OF NATURAL AND APPLIED SCIENCE**

**IDENTIFICATION OF MECHANICAL PROPERTIES OF GRAPHENE-EPOXY
NANOCOMPOSITES USING NANOINDENTATION TECHNIQUE**

OSMAN BAYRAK

**MASTER OF SCIENCE THESIS
DEPARTMENT OF MECHANICAL ENGINEERING
DESIGN PROGRAM**

**SUPERVISOR
PROF. DR. ÖZGEN Ü. ÇOLAK**

İSTANBUL, 2012

T.C.
YILDIZ TECHNICAL UNIVERSITY
GRADUATE SCHOOL OF NATURAL AND APPLIED SCIENCE

**IDENTIFICATION OF MECHANICAL PROPERTIES OF GRAPHENE-EPOXY
NANOCOMPOSITES USING NANOINDENTATION TECHNIQUE**

The thesis written by Osman BAYRAK in 04.05.2012 was accepted by the Department of Mechanical Engineering, Graduate School of Natural and Applied Science at Yıldız Technical University as **MASTER OF SCIENCE THESIS**, with the approval of the jury.

Thesis Supervisor

Prof. Dr. Özgen Ü. ÇOLAK

Yıldız Technical University

Jury Members

Prof. Dr. Özgen Ü. ÇOLAK

Yıldız Technical University

Doç. Dr. Deniz UZUNSOY

Yıldız Technical University

Doç. Dr. Halit S. TÜRKMEN

İstanbul Technical University

PREFACE

Nanocomposites have an important place in many engineering fields. As a reinforcing material, graphene has promising mechanical properties for composites.

Compared to tensile test, nanoindentation test is much proper for characterization of mechanical properties of nanocomposites, and also of many other materials. For this reason, many studies are being performed by many groups of scientists for the accurate determination of mechanical properties from nanoindentation tests.

Numerical modelling of nanoindentation is an essential part of the studies to understand the nature of nanoindentation, and derive analytical formulations for it. In this study, a method for determination of viscoplastic parameters from nanoindentation tests using numerical modelling was discussed. Also, it was attempted to make some contributions to the modelling of nanoindentation both for elastoplastic and viscoplastic materials.

I thank my family for their moral support and patience. I also present my thanks to my colleagues and professors in Naval Architecture and Maritime Faculty at Yıldız Technical University for providing me an amicable working environment and technical support throughout my master study.

I am grateful to my thesis supervisor, Prof. Dr. Özgen Ü. ÇOLAK, for her directive on studying such a promising topic and great support throughout the study.

May, 2012

Osman BAYRAK

TABLE OF CONTENTS

	Page
LIST OF SYMBOLS	vii
LIST OF ABBREVIATIONS	viii
LIST OF FIGURES.....	ix
LIST OF TABLES.....	xi
ABSTRACT	xi
ÖZET.....	xiv
CHAPTER 1	1
INTRODUCTION1	
1.1 Literature Summary	1
1.2 Purpose of the Thesis.....	3
1.3 Hypothesis	3
CHAPTER 2	4
GRAPHENE-EPOXY NANOCOMPOSITES4	
2.1 Composite Materials.....	4
2.2 Nanocomposites and Nanoparticles.....	5
2.2.1 Graphene	7
2.2.1.1 Synthesis of Graphene	10
2.3 Epoxy.....	11
2.4 Graphene-Epoxy Nanocomposites and Their Production	11
CHAPTER 3	14
NANOINDENTATION TECHNIQUE14	
3.1 Characterization of Mechanical Properties of Materials.....	14

3.2	Hardness Testing Methods and Evolution of Nanoindentation Technique	15
3.2.1	Hardness Testing Methods.....	15
3.2.2	Theoretical Establishment of Macro-Scale Hardness Testing.....	16
3.2.3	Micro-Scale Hardness Tests.....	18
3.2.4	Nanoindentation Technique.....	18
CHAPTER 4	24
NUMERICAL MODELLING OF NANOINDENTATION24		
4.1	Introduction	24
4.2	Building and Verification of the Numerical Model	25
4.2.1	Constitutive Model for the Elastoplastic Material	26
4.2.2	Determination of the Geometry of the Sample	27
4.2.3	Investigation of the Tip Bluntness Effect.....	30
4.2.4	Effect of Element Type	32
4.2.5	Effect of Mesh Refinement in the Contact Region.....	33
4.2.6	Conclusion on the Verification Stage	33
4.3	Viscoplastic Numerical Modelling of Nanoindentation.....	34
4.3.1	Experimental Work.....	34
4.3.2	Forward Analysis	39
4.3.2.1	Constitutive Model for the Elastoviscoplastic Material.....	39
4.3.2.2	Determination of Viscoplastic Parameters of Pure Epoxy.....	39
4.3.2.3	Numerical Simulations for Forward Analysis.....	42
4.3.2.4	Conclusion on the Forward Analysis.....	49
4.3.3	Reverse Analysis	49
CHAPTER 5	53
RESULTS AND DISCUSSION53		
REFERENCES..... 55		
CURRICULUM VITAE		
		62

LIST OF SYMBOLS

P	Power
m	Mass
v	Speed
H	Hardness
σ_u	Ultimate tensile strength
P_m	Mean pressure
h_p	Plastic deformation depth
h	Depth at maximum load
P	Load
E	Young's modulus
E_r	Reduced Young's modulus
h_e	Elastic deformation depth
h_c	Contact distance
A	Projective area
ε^e	Elastic strain
ε^{pl}	Plastic strain
$\dot{\varepsilon}^e$	Elastic strain rate
$\dot{\varepsilon}^{vp}$	Viscoplastic strain rate
\mathbf{S}	Compliance matrix
\mathbf{s}	Deviatoric stress tensor

LIST OF ABBREVIATIONS

CNT	Carbon nanotube
SWCNT	Single-walled carbon nanotube
MWCNT	Multi-walled carbon nanotube
FEA	Finite element analysis
GPL	Graphene platelet
CVD	Chemical vapour deposition
GO	Graphene oxide

LIST OF FIGURES

		Page
Figure 2.1	Five allotropes of carbon: a) Diamond, b) Graphite, c) C60 (Buckminsterfullerene or buckyball), d) Amorphous carbon, and e) Carbon nanotube [38]	6
Figure 2.2	Graphene: a) wrinkled structure [49], b) single layer [50], c) Schematic representation, d) Bond structure of a graphene cell [51]	9
Figure 2.3	Thermal reduction (or functionalization) of GO	10
Figure 2.4	Schematic representation of 0.1 wt. % GPL-Epoxy nanocomposite.....	12
Figure 3.1	Schematic representation of an instrumented tester and Berkovich tip on a sample	19
Figure 3.2	Schematic of indentation with an ideal sharp conical indenter (lines having different thicknesses show the position of indenter).....	21
Figure 3.3	Typical load-displacement curve.....	22
Figure 4.1	Specimen models; a) with square geometry, and b) with proposed geometry, shown with displacements on the edges	28
Figure 4.2	Comparison of experimental and numerical analysis results of nanoindentation on Al 2024-T351, from geometrical aspect.....	29
Figure 4.3	Comparison of the models in terms of node numbers, using the proposed model.....	30
Figure 4.4	Indentation site showing the indenter: a) with sharp tip, and b) with blunt	31
Figure 4.5	Comparison of the models in terms of tip roundness	31
Figure 4.6	Comparison of the models in terms of element types.....	32
Figure 4.7	Comparison of the models in terms of mesh refinement around contact region.....	33
Figure 4.8	Load-displacement curves for pure epoxy (provided by Prof. Dr. Özgen Ü. ÇOLAK)	34
Figure 4.9	Load displacement curves for 0.1 wt. % fraction GPL-epoxy Nanocomposite [87]	36
Figure 4.10	Stress-strain curves for pure epoxy and GPL-epoxy Nanocomposites [85].....	37
Figure 4.11	Stress-strain curve for pure epoxy at different loading rates [88].....	38
Figure 4.12	Tensile curves after neglecting the viscoelastic behaviour (for the original graph, see Figure 4.11)	40
Figure 4.13	Finite element model of a Berkovich indentation: a) Volume of	

	the sample, which is generated by sweeping the 2-D sample model. b) Detailed image of Berkovich indenter on the sample	43
Figure 4.14	Mesh pattern of Berkovich indentation: a) Top of the sample, that is around the indentation site; b) Bottom of the Berkovich tip, showing the similar element distribution to the one on the sample; c) Element distribution on the Berkovich indenter (from a different point of view)	44
Figure 4.15	Comparison of load-displacement curves of conical, Berkovich nanoindentation simulations and experiment at a displacement rate of 200 nm/s on pure epoxy	45
Figure 4.16	Von Mises stress distribution around indentation site on pure epoxy sample, at peak load, for Berkovich indentation	46
Figure 4.17	Von Mises stress distribution around indentation site on pure epoxy sample, at peak load, for conical indentation.....	46
Figure 4.18	Contour of total displacement around indentation site on pure epoxy sample, at peak load, for Berkovich indentation.....	47
Figure 4.19	Contour of total displacement around indentation site on pure epoxy sample, at peak load, for conical indentation.....	47
Figure 4.20	Comparison of the load displacement curves of the numerical models and experiment on pure epoxy at displacement rate of 200 nm/s	48
Figure 4.21	Comparison of the load displacement curves of the numerical models and experiment on pure epoxy at displacement rate of 20 nm/s.....	49
Figure 4.22	Comparison of the load-displacement curves of experiments and numerical models that were given various viscoplastic parameters, which were conducted for 0.1 wt. % fraction GPL-epoxy (The curves having thick and dashed lines are those providing approximate m and γ values. The experimental curves are modified to make the graph clearer, see the Figure 4.9 for the original curves)	51

LIST OF TABLES

	Page
Table 2.1 Comparison of effects of nanoadditives on enhancement of fracture toughness and fracture energy of pristine epoxy [8].....	9
Table 4.1 Yield stresses, determined using 0.002 offset rule and applying common intersection, corresponding to each strain rate for pure epoxy	40
Table 4.2 Peak load values (in Newton) obtained from the simulations (blue coloured values show that they are between the experimental values).....	52

**IDENTIFICATION OF MECHANICAL PROPERTIES OF GRAPHENE-EPOXY
NANOCOMPOSITES USING NANOINDENTATION TECHNIQUE**

Osman BAYRAK

Department of Mechanical Engineering

Master of Science Thesis

Supervisor: Prof. Dr. Özgen Ü. ÇOLAK

Developing technology let society use more sophisticated materials by which better performance is gained in many fields of application. Composite materials are some of those associated materials. While they provide with lighter devices, vehicles etc., they decreases the amount of energy to be consumed.

Thanks to its strong C-C bonds, carbon-based materials are some of the mostly used reinforcement phases in composites. Especially when they are synthesized to nano sizes, better results are observed in the matrices where they are added.

Graphene has the unrolled form of carbon nanotubes which has great mechanical properties. It usually exists in the form of agglomeration of plates rather than a single layer. When it is produced as single or several layers, it exhibits better performance and transfers its excellent properties to the matrix better than single walled carbon nanotubes do.

The factors such as relatively high production costs, and use of nanomaterials and any other technological materials as coating besides as structural elements make tensile test a challenging method for material characterization. Nanoindentation test is a good

solution for such constraints. Compared to a tensile test, very small and less numbers of specimens are enough for a nanoindentation test.

Although much progress has been made, more steps are needed to be taken for the exact determination of stress-strain curves using nanoindentation tests, which is originally gained from tensile tests.

In this study the determination of viscoplastic material properties of a graphene-epoxy nanocomposite, of which the production and the nanoindentation experiments was performed by the thesis coordinator Prof. Özgen Ü. ÇOLAK, and Ardavan ZANDIATASHBAR, using the tests and numerical models of nanoindentation were researched.

This thesis consists of five chapters. After giving a literature abstract, purpose of the thesis, and hypothesis in the first chapter, a detailed literature review on the material, and the method were presented in the second and third chapters, respectively. In the fourth chapter, the method of determination of viscoplastic parameters using nanoindentation was introduced. Finally, the results were discussed in the last chapter.

In the second chapter, brief information about the structure, properties and various synthesis methods of graphene, epoxy and graphene/epoxy nanocomposite were given. Advantageous and disadvantageous of graphene compared to other carbon based nano materials were explained.

Third chapter covers the emergence of nanoindentation technique, and the theoretical base of nanoindentation to obtain young's modulus. Beginning with Brinell, hardness measurement techniques and then theories developed to explain the indentation contact were indicated. The contributions done to the method of derivation of Young's modulus were provided in accordance with the dates of the works. Applicability of the method for viscoplastic materials was stated.

In chapter four, method of derivation of viscoplastic material properties of graphene-epoxy nanocomposite using nanoindentation tests and numerical simulations was examined and positive results were gained. While examining this method some determinations were done on the numerical modelling of nanoindentation.

Results were briefly discussed in the chapter five.

Keywords: Graphene-epoxy nanocomposite, viscoplastic material, nanoindentation process, finite element method.

**NANOİNDENTASYON YÖNTEMİ İLE GRAFİN-EPOKSİ
NANOKOMPOZİTLERİN MEKANİK ÖZELLİKLERİNİN BELİRLENMESİ**

Osman BAYRAK

Makine Mühendisliği Bölümü

Yüksek Lisans Tezi

Tez Danışmanı: Prof. Dr. Özgen Ü. ÇOLAK

Gelişen teknoloji, topluma birçok alanda gün geçtikçe daha üstün performanslar sergileyen ileri malzemeler kullanma imkanı tanımaktadır. Kompozit malzemeler de söz konusu malzemeler sınıfında yer almaktadır. Kullanıldıkları araç ve gereçlerde hafiflik sağlamalarının yanı sıra, enerji tüketiminin azaltılmasında da büyük rol oynarlar.

Sahip oldukları güçlü karbon-karbon bağları sayesinde karbon temelli malzemeler kompozitlerde en sık kullanılan takviye elemanlarından. Özellikle nano boyutta sentezlenen parçacıklar katıldıkları matrislerde çok daha iyi sonuçlar verirler.

Grafin tek duvarlı bir karbon nanotüpün açılmış haline benzer bir yapıya sahiptir. Tekil bir katman halindense daha çok plaka yığınları halinde mevcuttur. Ancak tek veya birkaç bir plaka şeklinde sentezlendiklerinde tek duvarlı karbon nanotüplerden daha iyi bir biçimde mekanik özelliklerini matrislere aktarırlar.

Nano malzemelerin nispeten pahalı olması, yapı elemanı olarak kullanılmasının yanı sıra kaplamada da kullanılmaları gibi sebeplerden dolayı, malzeme karakterizasyonunun çekme deneyi ile yapılması zordur. Nanoindentasyon testleri bu tür zorluklara bir çözüm olarak ortaya çıkmıştır. Çekme testleri ile kıyaslandığında çok küçük boyutlarda ve miktarlarda numuneler test için yeterli olabilmektedir.

Her ne kadar birçok ilerleme kaydedildi ise de, normalde çekme testinden elde edilen ve malzemenin mekanik özellikleri hakkında bilgi veren gerilme-gerinim eğrisinin

nanindentasyon testi ile kesin tespiti için daha çok çalışmaların yapılması gerekmektedir.

Bu tez çalışmasında üretimi ve nanindentasyon testleri tez yürütücüsü Prof. Dr. Özgen Ü. ÇOLAK ve Ardavan ZANDIATASHBAR tarafından gerçekleştirilen grafin-epoksi nanokompozitlerin viskoplastik malzeme özelliklerinin nanindentasyon testleri ve sayısal modellemeleri yolu ile tespit edilmesi araştırılmıştır.

Tez beş bölümden oluşmaktadır. İlk bölümde literatür özeti, tezin amacı ve hipotez verildikten sonra ikinci ve üçüncü bölümlerde söz konusu malzeme ve yöntem hakkında detaylı bir literatür taraması sunulmuştur. Dördüncü bölümde nanindentasyon ile viskoplastik parametre tespit yöntemi anlatılmıştır. Beşinci bölümde sonuç ve öneriler sunulmuştur.

İkinci bölümde ilgili malzeme hakkında genel bilgiler verilmiştir. Grafin, epoksi ve grafin-epoksi nanokompozitin yapısı, özellikleri ve çeşitli sentezleme yöntemleri hakkında kısa bir bilgilendirme yapılmıştır. Grafinin diğer karbon temelli nano malzemelerle kıyaslandığında sahip olduğu artılar ve eksiler anlatılmıştır.

Nanindentasyon tekniğinin ortaya çıkışı ve elastisite modülünün tespiti için kullanılan nanindentasyonun teorik temeli üçüncü bölümde ele alınmıştır. Brinell' den başlayarak sertlik ölçme tekniği ve indentasyon kontağını açıklamak için geliştirilen teoriler açıklanmıştır. Elastisite modülü tespit yöntemine yapılan katkılar çalışmaların tarihsel sırasına göre anlatılmıştır. Söz konusu yöntemin viskoplastik malzemelere uygulanabilirliği ifade edilmiştir.

Dördüncü bölümde grafin-epoksi nanokompozitin nanindentasyon testleri ve nanindentasyonun sayısal benzetimleri kullanarak viskoplastik malzeme özelliklerini tespit yöntemi tahlil edilmiş ve olumlu sonuçlar elde edilmiştir. Yöntemin tahlili sırasında nanindentasyonun sayısal modellemesi ile ilgili bir takım tespitlerde bulunulmuştur.

Beşinci bölümde, yapılan çalışmalarda elde edilen sonuçlar özet biçiminde anlatılmıştır.

Anahtar Kelimeler: Grafin-epoksi nanokompozit, viskoplastik malzeme, nanindentasyon prosesi, sonlu elemanlar yöntemi

INTRODUCTION

1.1 Literature Summary

It has been widely accepted that nanocomposites exhibit better performance compared to conventional composites [14].

Discovery of CNTs opened an era in the field of nano science and many efforts have been made to enhance carbon-based nano materials[5].

In 1947, graphene was discovered as the building block of graphite by Wallace [6].It was not until 2004, when synthesis of single graphene sheet was achieved [7], that it was realized that graphene could be useful for nanocomposite applications. Rafiee et al. reported that graphene platelets enhance the mechanical properties of nanocomposites better than carbon nanotubes do, even when graphene was used ten times less [8].For the production of bulk quantity of graphene, chemical and thermal reduction was reported to be the best method [9],[10].

The systematic hardness testing technique was invented by Brinell in 1900 [11]. Meyer used projected area rather than surface area of indent, that is used in Brinell' s formulation [12]. In 1914, Rockwell suggested an indenter geometry which provides easy and fast measurement of projected area [13]

Four faceted diamond indenter was first used by R. L. Smith and G. E. Sandland to enhance Brinell' s method as to be used for harder materials and provide less destruction [14].

First correlation between the hardness and stress-strain diagram, or ultimate tensile strength, was made by Brinell [11].

Tabor [15] built up a theoretical basis for hardness measurement using the Hertz's [16] approach for elastic deformation of contacting spherical bodies. Using the plastic deformation models for non-hardening materials [17-19], Tabor developed a relationship between mean pressure and yield strength [20].

Very shallow indents, as small as 20 nm, was performed by Pethica et al. [21]. Bulychev et al. [22] measured elastic modulus from indentation experiments.

Elastic displacement of sample indented was related to elastic modulus by Doerner and Nix [23]. Sneddon's solution [24] was the basis of the work of Doerner and Nix.

Three faceted pyramidal diamond indenter was invented by Berkovich [25] for a more sensitive indentations at small depths.

Oliver and Pharr [26] improved the method, which was proposed by Doerner and Nix, by using the Sneddon's study for conical indenters.

Jayaraman et al. [27] proposed a method to obtain characteristic plastic strain of geometrically similar indents. Using characteristic plastic strain-cone angle correlation and relation of hardness-flow stress, they derived stress-strain curves of a steel from nanoindentation tests.

Huber and Tsakmakis [28] developed an inverse method to determine stress-strain curves from nanoindentation tests.

Benefiting from numerical simulations, Giannakopoulos & Suresh [29] presented a methodology to extract stress-strain curves from nanoindentation tests. Distinctive side of their study was that they made a unique correlation between the indentation depth and contact area taking the pile-up and sink-in into consideration.

Tunvisut et al. [30] developed an elastic plastic material property extraction method from nanoindentation tests. They proved that elastic modulus is independent of indentation depth while yield strength is highly dependent of the depth of penetration.

Beghini et al. [31] extracted stress – strain curves of a group of metals using finite element analysis of indentation with an optimization algorithm. By fitting a continuous function to load displacement curve that was gained from numerical simulations, they obtained load displacement curve from constitutive parameters. So, they could apply an optimization algorithm to deduce stress-strain curve from nanoindentation tests.

Kim et al.[32] made a representative stress and strain approach to derive stress-strain curves of ten different metallic materials from load-displacement curves.

Huber *et al.*, and Ullner *et al.* gained viscoplastic material properties using neural network based analysis method [33],[34].

1.2 Purpose of the Thesis

In this thesis, it was aimed to examine if nanoindentation process can be employed for viscoplastic material characterization. While studying this method, some contributions were attempted to make to the numerical modelling of nanoindentation.

1.3 Hypothesis

Viscoplastic parameters of a nanocomposite and of any quasi-homogeneous isotropic material can be determined using numerical simulations of nanoindentation in accordance with nanoindentation tests, without needing any ambiguous tensile tests at different loading rates.

GRAPHENE-EPOXY NANOCOMPOSITES

2.1 Composite Materials

Energy efficiency is one of the most important phenomena in recent decades. Decrease in fossil fuel resources, which are the main energy supply for today's industry and vehicles, and harmful effects to the environment arising from use of these fuels let humankind use environmentally friendly energy resources. Ways to benefit from these resources can be counted as generating renewable energy converting systems and improvement of these systems in terms of efficiency. Arising question from here is how to improve efficiency.

Giving speed to a mass requires power ($p = mv$). As we lessen the mass, we increase efficiency. Blades of windmills, chassis of an automobile are examples for this situation. Lesser weight they have, more speed they reach, by the same source of power. Considering the equation given above, we conclude that we have to decrease the mass (m) if we want to reach the same speed with lesser power or greater speed with the same power.

There are two ways to decrease the mass. First, using thinner, smaller sizes of the same material; and second, altering the material with the lighter material which also has the same strength with the previous material. The first is mostly undesirable, so the latter is the solely applicable way.

Composite materials are those which provide us relatively lighter and stronger structures, machine parts, shields etc. While these materials give lightness to

structures, they can also improve the other capabilities of the structures such as thermal resistivity or thermal conductivity and electrical resistivity, conductivity or semi conductivity.

Composite materials (or shortly composites) consist of two or more materials that are physically and/or chemically different from each other. Some composites are naturally occurred such as sand, mud and woods. Composites are generally made of a matrix and additives. The additives can be counted as particles, fibres and laminates etc.

Depending on their content, they get titles. Composites with laminates are named as laminate composites, those with fibre reinforcement additives are titled as fibre composites. Likewise, composites containing nanoparticles are called nanocomposites.

2.2 Nanocomposites and Nanoparticles

Nanocomposites are the composites which contain nanoparticle additives having a size less than 100 nm at least in a dimension. Developing technology provide means to acquire nano-sized objects. The reason of focusing on nanoparticles is that they comprise properties such as more homogeneous distribution (when some special methods are applied) [13] and better surface contact with matrix [4].

Knowing the power of carbon-carbon bonds, scientists are studying intensely on the carbon-based materials. As is known, diamond, which is composed of carbon atoms, is practically the strongest material in the world. As diamond, graphene (name of each single layer of graphite), is also an allotrope of carbon element. Some other allotropes of carbon can be counted as fullerene (C₆₀), carbon nanotubes (CNTs), amorphous carbon. Compared to diamond, since they are relatively cheap, fullerenes, carbon nanotubes, and graphenes are preferred as additives for composite materials.

Ever since it was discovered in 1991 [5], many efforts has been made on the study of CNTs. Besides having an elasticity modulus of about 1 TPa [35] and strength reaching to 63 GPa [36], small diameter and great length to diameter ratio give CNTs capability to transfer their extreme mechanical properties to the matrix in which they are involved [37]. CNTs can be visualized as the rolled form of single graphene sheet, which

has the dimension with wall thickness of 0.334 nm, diameter of order of 100 nm and length ranging between 20 and 100 μm .

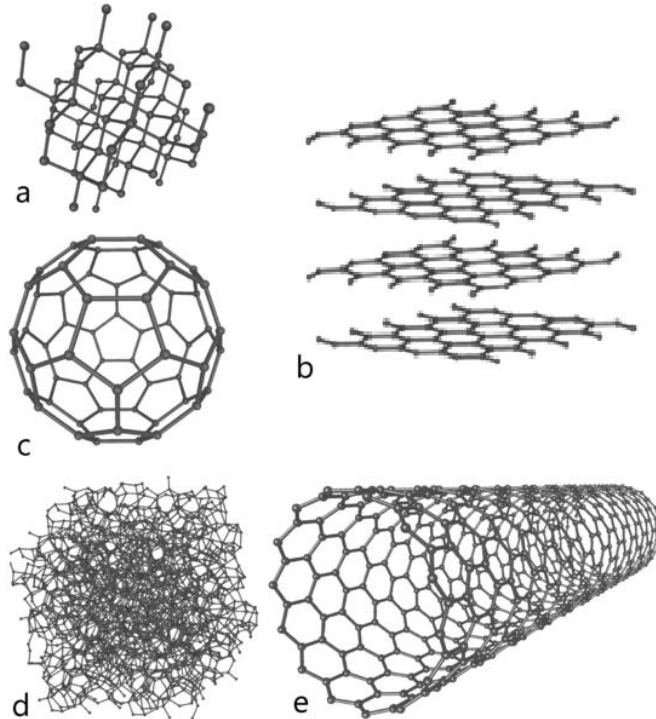


Figure 2.1 Five allotropes of carbon: a) Diamond, b) Graphite, c) C₆₀ (Buckminsterfullerene or buckyball), d) Amorphous carbon, and e) single-walled carbon nanotube [38]

CNTs are classified into three [37]; single walled carbon nanotubes (SWCNTs), multi-walled carbon nanotubes (MWCNTs) and carbon nanofibers (CNFs). CNTs own their characteristic mechanical properties (and also electrical and thermal properties) depending on their atom arrangement [39]. Although production costs are low for MWCNTs compared to that of SWCNTs [37], weak Van Der Waals bonds between the layers of MWCNT, which may cause slippage inside the matrix due to the applied stresses, make MWNTs weak fillers for composites [2].

When incorporating CNTs into matrix, some difficulties are encountered like non-homogeneous distribution caused by high viscosity due to “bird’s nest” structure of CNTs [40] and occurrence of CNT bundles, that leads to weaknesses for composite, due to the van der Waals interactions. However, many methods, such as covalent

functionalization and polymer grafting of CNTs, are presented in the literature to overcome non-homogeneity [3],[36],[38].

Although carbon-based nanoparticles have excellent mechanical properties besides electrical and thermal properties, their small-scale size prevent application of them directly into practice in the macro-scale with today's technology, which only let them to be used in matrices as additives to produce composites.

Basically, their high aspect ratio, intrinsic strength and large interaction area per unit mass make carbon-based nanomaterials best candidate for nanocomposites.

For the characterization of mechanical properties of nano-sized bodies, MD (molecular dynamics) simulation, FEA, experimental and theoretical methods can be used. MD simulations are especially employed in cases where boundary conditions cannot be satisfied in experimental setups [41].

2.2.1 Graphene

Though it is the last several years when many scientific studies have been conducted, the discovery of graphene dates back to 1947 [6]. Since it was found, by Geim *et al.* in 2004, that graphene sheets can be synthesized in the form of single layer (or few layers) [7], scientific studies have focused on this material. Difficulties in synthesis [42] and high viscosity when compounded with polymers, were disadvantageous properties of CNTs for the use of them as nanoparticle reinforcement material. In addition to young's modulus of 1 TPa and high strength reaching to 130 GPa [43], 2-D structure with one atom thickness, wrinkled surfaces [44], cost-effective production [40], large surface area/volume ratio (or specific surface area) and higher glass transition temperature in composites [44] are the prominent features of graphene over other carbon nanoparticles.

Carbon atom, which is the building block of graphene, has six electrons with configuration $1s^2 2s^2 2p^2$. As it can be seen from the configuration, carbon atom has four valence electrons. Graphene is composed of sp^2 bonded carbon atoms, where three electrons are shared and one electron is free for each atom. Thanks to this free electron, graphene can conduct electricity. In contrast to graphene, diamond has no

free electrons because each carbon atoms have covalent bonds with four carbon atoms, remaining no free electron. Therefore, diamond cannot conduct electricity.

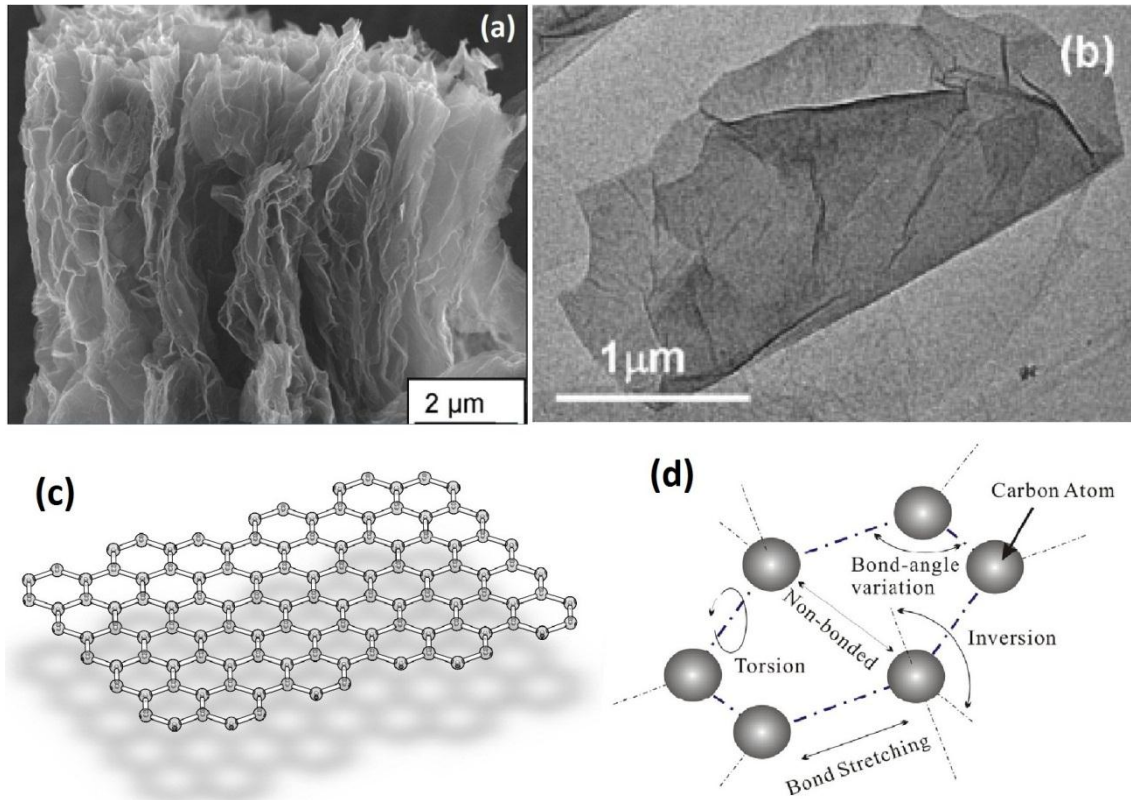
Three carbon atoms, which is covalently bonded to one carbon atom lead to a honeycomb structure in graphene. Due to this structure mechanical properties of graphene are direction dependent. For instance, poisson ratio ranges between 1.441 and 1.129 relative to direction of displacement [45]. Since graphene has one atom thickness it is assumed as 2-dimensional. This 2-D structure is actually the most distinctive property of graphene compared to CNTs, mechanical properties of which is almost identical with that of graphene. Thanks to its 2-D structure, both surfaces of graphene contact to the matrix, so that it can transfer far better its intrinsic properties to the matrix. Experiments reported in the literature prove this. By compounding functionalized SWCNTs with 1% weight into epoxy, ~30% increase in young's modulus and ~15% increase in strength is observed [46]. Surprisingly, by adding functionalized graphene with only 0.1% weight into epoxy much better enhancements in mechanical properties such as ~31% increase in modulus and ~40% increase in strength are obtained [8].

Wrinkled surface [47] inherent to graphene has another factor on enhancement of mechanical properties of composites. Mechanical interlocking which is vital for load transfer is provided due to the wrinkled surface of graphene [44]. Roughness caused by wrinkled structures acts within matrix like dislocations in metals. In other words, wrinkles constraint movement of shear bands to some extent.

Since graphene is building block of graphite which is readily available in nature, its production costs are very low, especially when compared to CNTs. By applying one of several graphene synthesis methods such as chemical reduction or thermal reduction, bulk quantity of graphene sheets can easily be synthesized [9],[10].

Thickness of a single graphene sheet is about 0.34 nm and its length and width vary between 1 μm and 300 μm . Considering graphene platelets (GPLs) as they have several layers and interspacing of 0.72 nm between layers, the thickness of GPL is about 1.5 nm [8]. Even with this thickness, aspect ratio of GPL (hereafter the term GPL will be used to distinguish graphene platelets from monolayer graphene) may reach to

200000. To compare with graphene, CNTs has aspect ratio of 1000 [48]. Aspect ratio has an important factor on lessening the fatigue crack growth in composites. It is indicated in Table 2.1 that GPLs exhibit better performance on enhancement of fracture toughness and fracture energy.



2.2 Graphene: a) wrinkled structure [49], b) single layer [50], c) Schematic representation, d) Bond structure of a graphene cell [51]

Table 2.1 Comparison of effects of nanoadditives on enhancement of fracture toughness and fracture energy of pristine epoxy [8]

Sample Type	Fracture Toughness, K_{Ic} ($\text{MPa m}^{1/2}$)	Fracture Energy, G_{Ic} (J/m^2)
Pristine Epoxy	0.96 ± 0.047	251.3 ± 19.03
Epoxy/MWCNT-at 0.1 wt.%	1.15 ± 0.131	417.8 ± 30.83
Epoxy/SWCNT- at 0.1 wt.%	1.1 ± 0.117	365.7 ± 25.37
Epoxy/GPL- at 0.1 wt.%	1.48 ± 0.183	567.2 ± 29.17

2.2.1.1 Synthesis of Graphene

For the synthesis of GPL, there exist several methods. Those are epitaxial growth of graphene sheets on silicon carbide (SiC) [52], chemical vapour deposition (CVD) on nickel surfaces [53], mechanically exfoliating graphene layers using scotch tape [7], reduction of graphene oxide [54]. The last method is the most suitable one for the synthesis of bulk quantities of GPL. Here, in this study, the method of thermal reduction of graphene oxide, which is also utilized for the manufacturing of specimens that is used for the experiments mentioned in this study, is explained.

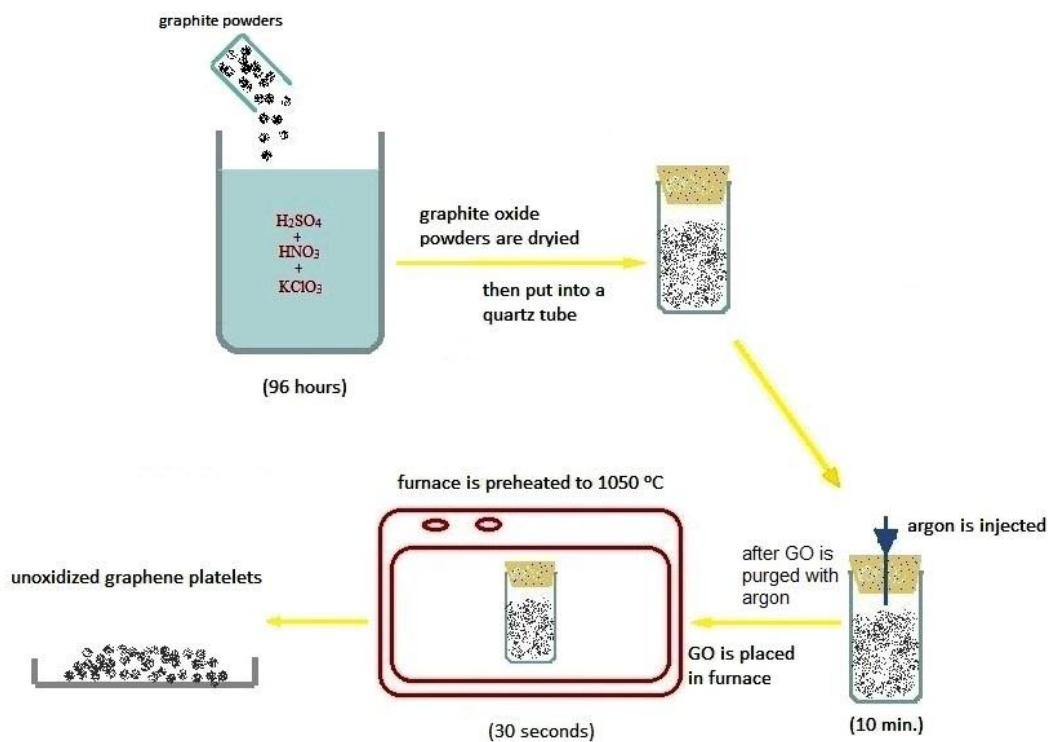


Figure 2.3 Thermal reduction (or functionalization) of GO

In the thermal reduction process, graphite oxide is un-oxidized while separating it into single layers in a furnace. Graphite oxide (GO) are obtained by oxidizing graphite in a solution of sulphuric acid, nitric acid, and potassium chlorate for more than 96 hours [55]. After drying the solution, GO powders are placed in a quartz tube then tube is closed by a stopper. Through the stopper, argon is injected to purge GO for 10 min. For splitting GO into single layers, quartz tube is quickly put into a tube furnace heated rapidly (>2000 °C /min) to 1050 °C and hold in the furnace for 30 s [47], so that graphene platelets are obtained.

2.3 Epoxy

Epoxy resin is one of the strongest polymers. For this reason, it is widely chosen for structural purposes. Epoxy is a thermoset formed from the reaction of epoxide (bisphenol A is used for the specimen) with curing agent polyamine. With the mix of these compounds, covalent bonds are formed between epoxide groups and amine groups. Since many covalently bonded crosslinks occur between each group of the compounds, resulting polymer is very strong. Due to its simple application procedure and great strength relative to other polymers, epoxies have wide range of application areas such as aerospace and automotive industries, marine applications, and electronics component coverings.

Unless GPLs or graphenes chemically functionalized, there exist no chemical bonding between epoxy matrix and GPLs [56],[57]. Some of the studies have shown that modification, although some decreases in strength of GPLs observed, enhances the mechanical properties of the nanocomposites [37].

2.4 Graphene-Epoxy Nanocomposites and Their Production

As mentioned earlier, nanoparticles, having great mechanical, thermal, and electrical properties cannot be directly applied in macro-scale in today's technology. Rather, they are employed to upgrade the properties of materials that are applicable in macro-scale. Therefore, nanocomposites are emerged for the possible use of aforementioned nanoparticles.

Epoxy, which is used in the places where high level strength/mass ratio is needed, is strengthened best by compounding it with graphene platelets (GPLs) [43],[5864].

Epoxy has wide variety of kinds formed depending on their compounds used and/or processing technique applied during compounding. The one used in this study has a tensile strength of 34.8 MPa and modulus of 2.77 GPa [65]. The previous studies indicated that the GPL of 0.1 % is the best fraction for toughening epoxy at maximum level [66]. When 0.1% GPL is incorporated into epoxy, 3% increase in modulus and 19% increase in yield strength were obtained [65]. Enhancement values are highly affected by manufacturing conditions. Due to this, the results given above are different than

the results reported by Rafiee *et al.* Also the infused particles help to decrease brittleness of host material, i.e. epoxy is very brittle. Any crack formed during loading suppressed when propagating crack encountered with GPLs [66].

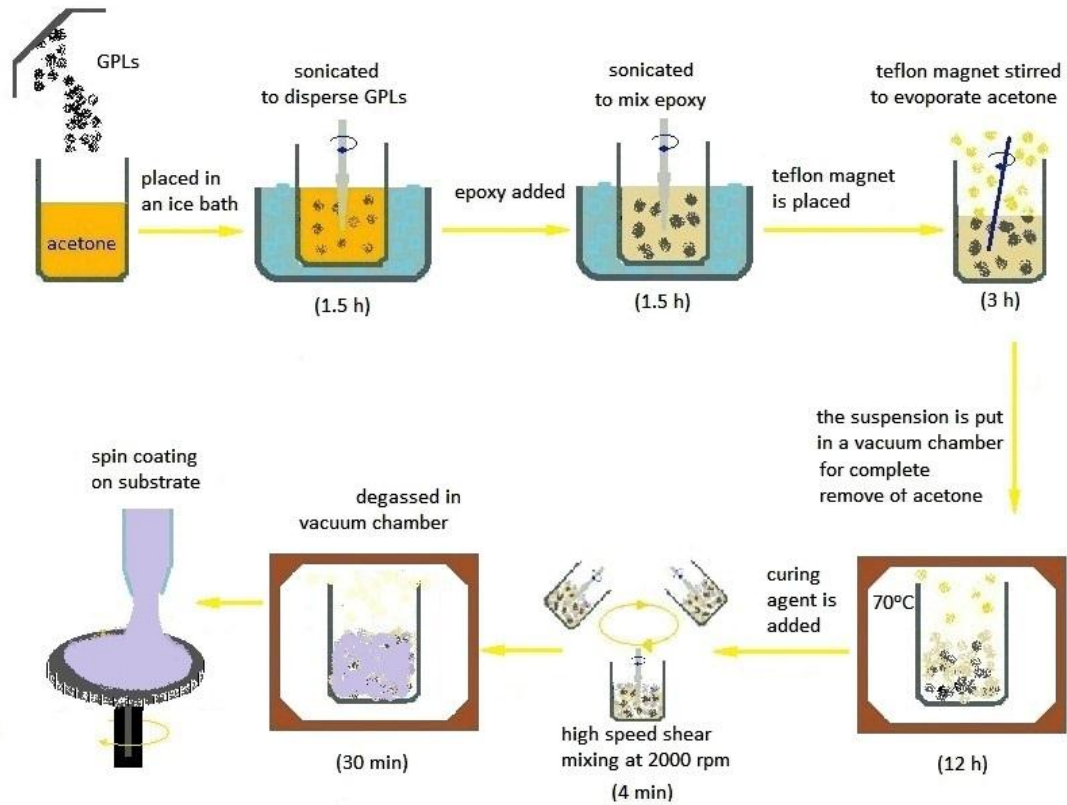


Figure 2.4 Schematic representation of 0.1 wt. % GPL-Epoxy nanocomposite

For manufacturing 0.1 wt. % graphene/epoxy nanocomposite, the following procedure is applied. Previously prepared GPLs are poured into acetone with the rate of acetone of 100 ml per GPL of 0.1 g. The mixture is sonicated for 1.5 h in an ice bath to disperse GPL in acetone. Epoxy resin (bisphenol-A) is added to the mixture and the mixture is sonicated in the same way for 1.5 h. To remove acetone, the mixture is heated on a magnetic stir plate using a Teflon-coated magnetic bar for 3 h at 70 °C, and acetone is evaporated. The acetone should completely be removed from the mixture. To do this, the mixture is hold in a vacuum chamber for 12 h at 70 °C. Obtained graphene/epoxy suspension is cooled at room temperature. Next, a low viscosity epoxy curing agent is added to the suspension and mixed using a high speed shear mixer for 4 min at 2000 rpm. For degassing epoxy, the suspension is again placed in the vacuum chamber and hold for 30 min. Finally, the mixture is poured onto silicon substrates, and the

nanocomposite is cured at room temperature and under 6.2 bar pressure for 24 h, followed by 4 h of post-cure at 90 °C [47],[60].

NANOINDENTATION TECHNIQUE

3.1 Characterization of Mechanical Properties of Materials

In engineering design, basic mechanical properties of materials are inevitably needed beside many other design parameters. Basic mechanical properties of a material can be counted as modulus of elasticity (E), poisson ratio (ν), yield stress (σ_y) and strain hardening (or softening) parameters. Depending upon the type of the material, (e.g., bilinear, elastic-nonlinear plastic, viscoelastic, viscoplastic, elastic-viscoplastic, viscoelastic-viscoplastic, etc.) some additional properties exist as well.

For determination of the basic mechanical properties, classical tensile tests, also known as tension tests, are employed. Since almost all structures exposed to static loading, that is even when there is no load out of the structure's weight, the basic mechanical properties of a material are recognized as those derived from quasi-static tensile tests. For this reason, tensile test is the first step for characterizing materials' mechanical behaviour. Quasi-static tensile tests are conducted at rates varying between 10^{-5} s^{-1} and 10^{-3} s^{-1} .

Besides their basic, or quasi-static, mechanical properties, almost all materials have time-dependent properties such as creep behaviour, stress relaxation. For some materials, such as polymers or polymer based composites, time dependency is prominent. Therefore, tensile tests at different displacement and/or loading rates are performed to characterize time-dependent behaviour of materials. For such tests, rate may reach to $3 \times 10^3 \text{ s}^{-1}$.

Some other mechanical property characterization tests are compression, torsion, three-point bending, four-point bending, Charpy impact, and indentation hardness. All the tests can also be performed under different thermal conditions to quantify temperature dependence of the materials' behaviour.

3.2 Hardness Testing Methods and Evolution of Nanoindentation Technique

3.2.1 Hardness Testing Methods

Hardness is one of the characteristics of every solid material. The first systematic method to measure the hardness of materials was invented by J. A. Brinell in 1900 [11]. By pressing a hard steel ball on investigated material, dent is formed on the surface of the material. Brinell hardness is calculated as the applied force divided by the surface area of the created dent. That is;

$$BHN = \frac{2F}{\pi D(D - \sqrt{D^2 - d^2})} \quad (3.1)$$

where F , D , and d are the force applied, diameter of the indenter and the diameter of the resulting dent, respectively. Applied force is designated with kgf and varies between 3000 kgf and 500 kgf depending on the hardness of the indented material. The ball diameter is 10 mm and this is an undesired dimension due to the damage caused, but it is useful when a heterogeneous material is investigated. Constituent material of Brinell tip is generally hard steel, but those produced from tungsten carbide is employed for testing relatively hard materials. In 1908, Meyer [12] suggested a hardness scale similar to that of Brinell, but with a difference that area considered is projected area. The Meyers formulation gives mean pressure P_m which is widely used today in nanoindentation processes.

Rockwell test method is a much faster and less destructive method compared to Brinell. Both spherical and conic tips can be used. The angle of the used cone is 120° . The procedure to calculate the hardness is slightly different than that of Brinell. It was suggested by Professor P. Ludwik in 1908. Later, in 1914, it was first applied by H. M. Rockwell and S. P. Rockwell. What make Rockwell superior to Brinell are that Hardness

can be displayed as indentation performed due to the procedure where indentation area is directly calculated from penetration of the tip, and it causes very small deformation on the tested material [13].

In 1921, Vickers Method was enhanced by R. L. Smith and G. E. Sandland [14] with the aim of finding an alternative to the Brinell, of which, hardness calculations are dependent on the size of the tip, and application is limited due to the hardness of material investigated. In Vickers test, the indenter has such geometry where area of cross section normal to the penetration direction is proportional to the penetration length. Thus, geometrically similar dents could be made at any load or depth. A pyramid with equal diagonals at the base can satisfy such geometry. And also it is made of diamond to maximize the rigidity. The angle at the tip end was specified as 136° which was derived from the ideal size of Brinell impression that is $3/8$ of the diameter of Brinell ball. When tangents at the ends of a chord, calculated from the aforementioned ratio, were intersected, the angle of 135.95° ($\sim 136^\circ$) is obtained. Just like in Brinell, hardness is defined as the load divided by the surface area of indentation [14].

In 1939, Fredrick Knoop introduced a modified version of Vickers that is compatible for thin and/or brittle materials. Using Vickers and Knoop methods, hardness tests at micro-scale can be performed.

3.2.2 Theoretical Establishment of Macro-Scale Hardness Testing

First attempts to make a correlation between the hardness and stress-strain diagram are as old as Brinell's work. He correlated (hardness) H and σ_u (ultimate strength) with an empirical formula:

$$\sigma_u = cH \tag{3.2}$$

where $c = 0.346$ for wide range of carbon steels [11]. In 1934, O'neill studied the correlation to establish a theory and he concluded that theoretical relation between the H and σ_u is ambiguous [67].

At the indentation process, contact occurs between two bodies, one is the indenter and the other is sample. Due to this, contact phenomenon was needed to be handled. First contact problems were handled by David Tabor in 1939 [68]. His earliest study was the modelling the plastic deformation of asperities on the surfaces of two contacting cylinders. Tabor's one of the most important work was "A simple theory of static and dynamic hardness" [15] where he built up a theoretical basis for indentation process by "discussing the shallowing of spherical indentations on the removal of load, the measurement of dynamic hardness, and what he called 'a simple theory of hardness' "[69]. Although the shallowing phenomenon was previously reported [67], theoretical approaches to this phenomenon were made by Tabor considering the elastic contact deformation of spherical bodies modelled by Hertz [16].

In 1940s, plastic deformation models for indentation were developed [1719]. These models are prepared for non-hardening materials. Considering these models, Tabor performed some experiments and developed a relationship between mean pressure (P_m) and yield stress (σ_y) [20].

$$P_m \approx c\sigma_y \quad (3.3)$$

where $c = 3$. This equation is valid for soft metals with very low hardening.

Tabor reasoned that similar indentations would cause similar stress distribution. Thus, the indentation diameter (d). From his experiments on strain hardening metals, Tabor set an empirical relation:

$$\varepsilon = A \left(\frac{d}{D} \right) \quad (3.4)$$

where the equation works best if $A = 0.2$.

Tabor placed equation (3.4) in power law hardening equation:

$$\sigma = H \left[0.2 \left(\frac{d}{D} \right) \right]^n \quad (3.5)$$

to indicate the equation with mean pressure which is calculated due to the Meyer hardness:

$$P_m \approx cH[A\left(\frac{d}{D}\right)]^n \quad (3.6)$$

Applying these formulations to results of indentations made on mild steel and annealed copper and choosing the value of c as 2.8, Tabor derived stress-strain curves very close to the tensile test results.

Tabor also extended his formulation for the pyramidal and conical tips [70]. Although Tabor's work is not applicable to all materials, it is pertinent for metals and wide range of solids.

3.2.3 Micro-Scale Hardness Tests

Between 1950s and 1980s, as the material science developed, scientists investigated the materials in micro-scale. Hardness tests were performed in micro-scale, so that less power was needed for making indentations. The idea of deriving material properties from hardness tests rather than tensile tests progressed. Vickers indenter was widely used for micro-scale measurements on brittle and thin materials. Developments in electronics such as x-ray scattering, electron microscopy etc., enabled investigation of deformation behaviours of materials with micro-indentations.

3.2.4 Nanoindentation Technique

Great advances in screening and measurement technology prompted scientist to use less destructive methods to characterize materials with the indentation. Scientists could achieve to perform indentations with a depth of penetrations as small as 20 nm [21]. Therefore such tests were called nanoindentation, or instrumented indentation tests. The devices performing such tests were first built by individual researchers such as Newey *et al.*, Pethica *et al.*, Loubet *et al.*, and Wierenga *et al.* [21],[7173]. The testers they used were able to sense depths with high resolution, for this reason they were called depth-sensing instruments. Monitoring indentations after load was removed may cause errors in determining hardness due to the elastic recovery of the indents [74]. One of the advantageous of depth-sensing instruments over conventional microhardness testers is that depth-sensing instruments do not require monitoring

indentations after load was removed since they can indicate the penetration continuously and with a great accuracy.

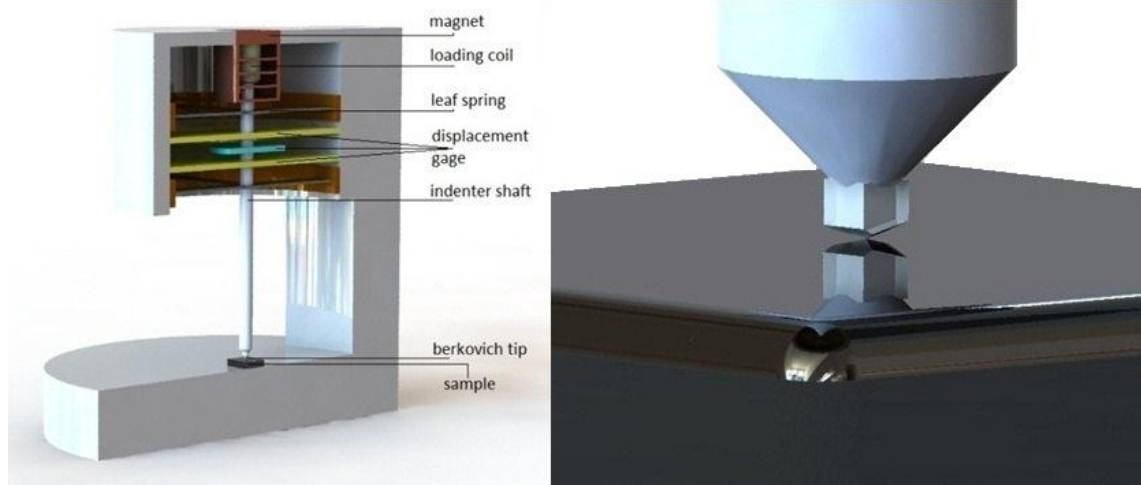


Figure 3.1 Schematic representation of an instrumented tester and Berkovich tip on a sample

Until 1970s, extracted mechanical properties from indentation tests were limited to ultimate tensile strength and hardness. In 1970s, several scientists measured elastic modulus from indentation experiments [22]. The test machines they employed were able to give continuous load-displacement data.

Doerner and Nix proposed a method relating elastic displacement of the sample to the elastic modulus [23]. They also suggested a hardness calculation technique which subtracts elastic displacement from total displacement. By knowing the geometry of indenter, cross-section, therefore projected indentation area, could be determined from the displacement of indenter. To calculate hardness, they took the plastic depth h_p , rather than total or final depth, which is determined by assuming a linear elastic recovery at the initial stage of unloading. This linearity is intersected at x axis, or displacement axis, so the resulting intersect is taken as plastic depth. They lent their assumption of linear elastic recovery on the observations on the metals they tested. To indicate plastic depth,

$$h_p = h - \frac{dh}{dP} P \quad (3.7)$$

where P is the maximum load applied and h is the depth at maximum load.

For the determination of modulus of elasticity, they proposed to use the unloading curve [23]. They also suggested making a flat punch approximation, which means no changes occur at the contact area during elastic recovery. With this assumption, they used adopted version of Sneddon's solution [24], made by Loubet *et al.* for a flat-ended cylindrical punch.

$$\frac{dh}{dP} = \frac{1}{2h_p} \sqrt{\frac{\pi}{24.5}} \frac{1}{E_r} \quad (3.8)$$

where

$$E_r = \frac{1 - \nu^2}{E} + \frac{1 - \nu_0^2}{E_0} \quad (3.9)$$

which was derived by Hertz.

Equation (3.8) is applicable to Berkovich indenter, because it is the geometrical equivalent of Vickers indenter. Berkovich indenter, which is mostly used for nanoindentation, was invented by E. S. Berkovich [75]. It has the best geometry for nano-scale measurements because three facets it has naturally intersect at a point. In contrast, Vickers pyramid has four facets and obtaining a single intersection point is very difficult for a body having four facets.

The methods, used today, to extract young's modulus from nanoindentation tests mainly based on Sneddon's study [76] where he applied Boussinesq's approach [77] for an indentation problem with a conical indenter to deduce load-penetration depth relationship,

$$P = \frac{2Etan\alpha}{\pi(1 - \nu^2)} h_e^2 \quad (3.10)$$

where, P , α , and h_e are applied load, half angle of indenter and rebound displacement of indenter, respectively.

Oliver *et al.* criticised the assumption of linearity at the initial stages of unloading, made by Doerner and Nix. They justified their criticism by the observations from the nanoindentation tests made on a number of materials. They used Sneddon's analytical solution [24], for cones and paraboloids of revolution rather than his flat punch

approximation which had been applied by Doerner and Nix [23],[26].

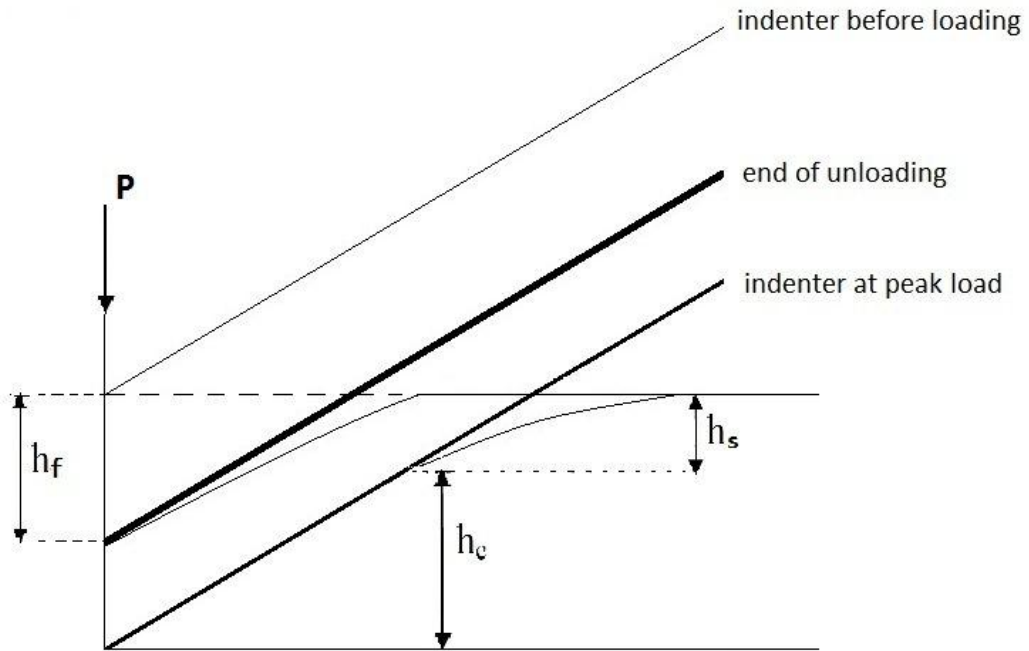


Figure 3.2 Schematic of indentation with an ideal sharp conical indenter (lines having different thicknesses show the position of indenter)

For the determination of E_r , according to Oliver-Pharr method,

$$E_r = \frac{\sqrt{\pi} S}{2 \sqrt{A}} \quad (3.11)$$

where S is initial unloading stiffness,

$$S = \frac{dP}{dh} \quad (3.12)$$

A is the function of h_c which is the vertical contact distance.

Since,

$$h_{max} = h_c + h_s \quad (3.13)$$

where h_{max} is the displacement of the tip at the maximum load, h_s was needed.

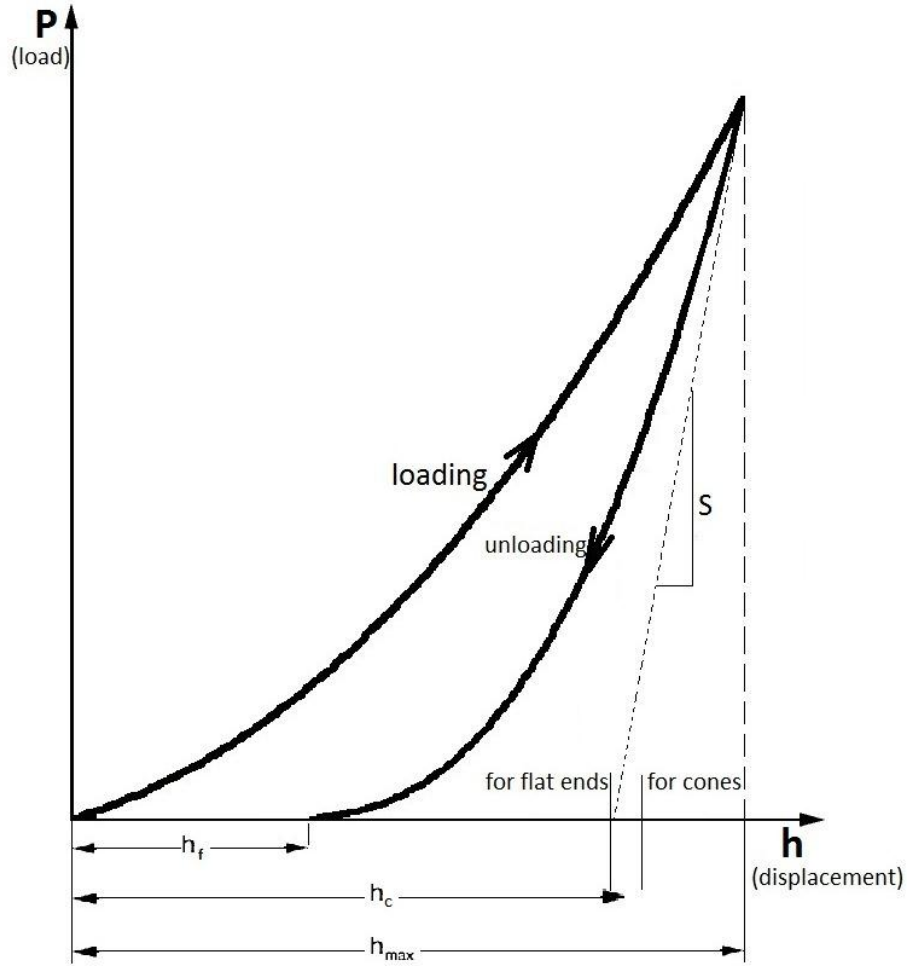


Figure 3.3 Typical load-displacement curve

From Sneddon's expression for conical indenter,

$$h_s = \frac{(\pi - 2) 2P}{\pi S} \quad (3.14)$$

After calculating h_s , h_c was found from the above equation (3.13) and placed in,

$$A = 24.5h_c^2 \quad (3.15)$$

When employed the Hertz equation, given above, E is obtained [26].

For more accurate estimation of elastic modulus, a correction factor γ was introduced into Equation (3.11) [78].

Jayaraman et al. [27] suggested a method to obtain characteristic plastic strain of geometrically similar indents. Also, they make a relation between hardness and flow stress of material. Using characteristic plastic strain-cone angle correlation and relation

of hardness-flow stress, they derived stress-strain curves of steel from nanoindentation tests.

Giannakopoulos & Suresh [29] identified a theoretical framework for nanoindentation tests. They presented a methodology to extract stress-strain curves from nanoindentation tests, benefiting from numerical simulations. Distinctive side of their study was that they made a unique correlation between the indentation depth and contact area taking the pile-up and sink-in into consideration.

Based on dimensional analyses and numerical simulations, Tunvisut et al. [30] developed an elastic plastic material property extraction method from nanoindentation tests. They also found that elastic modulus is independent of indentation depth. But, yield strength was highly dependent of the depth of penetration.

Beghini et al. [31] deduced stress-strain curve for a group of metals using finite element analysis of indentation with an optimization algorithm. To obtain load displacement curve from constitutive parameters, they fitted a continuous function to load displacement curve that they obtained from numerical simulations. So, they could apply an optimization algorithm to deduce stress-strain curve from nanoindentation tests.

Making a representative stress and strain approach, Kim et al.[32] derived stress-strain curves of ten different metallic materials from load-displacement curves which were obtained from indentation tests.

One major contribution to the material characterization using nanoindentation was made by Huber and Tsakmakis [28]. Using neural networks, they developed an inverse method to determine stress-strain curve from nanoindentation tests.

Huber *et al.*, and Ullner *et al.* gained viscoplastic material properties using neural network based analysis method [33],[34].

NUMERICAL MODELLING OF NANOINDENTATION

4.1 Introduction

As in the many fields of study, finite element method opens up ways for nanoindentation technique. Scaling and dimensional analysis keep an important place in modelling nanoindentation process and finite element method is widely used for dimensional analysis [79]. Also, using finite element method, some algorithms have been developed to obtain stress-strain curves of materials from nanoindentation tests [28].

Viscoplastic parameters are mostly determined using tensile tests at different loading rates. This process requires large amount of specimens and energy for running test machines. Here, in this work, with the aim of developing a fast and cost-effective viscoplastic parameter identification method, nanoindentation process was studied. As it has been explained in the third chapter, nanoindentation process is employed to determine material properties, especially for thin materials.

In this study viscoplastic parameters, viscosity and strain hardening exponent, of graphene epoxy were obtained by converging verified finite element model to the experimental results. This was called reverse process. Before doing this, a forward process has been carried out to check the applicability of the proposed technique. In the forward process, epoxy, of which tensile test results at different rates is known, was used. For an accurate finite element analysis, a verification step was conducted.

While conducting verification process some inferences have been made on numerical modelling of indentation.

4.2 Building and Verification of the Numerical Model

For an accurate and efficient finite element model, several factors were taken into account. These factors are geometry of the sample model, tip bluntness of the equivalent indenter, element type, mesh refinement in the contact region, and finally the indenter geometry.

As a geometrical equivalent of Berkovich indenter, conical indenter, having an apex angle of 70.3° , has been used for the analyses [80]. This equivalency was verified for elastoplastic materials [81]. Another confirmation to the equivalency was made by [82] where the ratio of the final indentation depth to the depth at peak load was above 0.65. Below this ratio, small differences between Berkovich indenter and conical indenter were reported. Since the aforementioned ratio for the material used in the verification came out far above the ratio of 0.65, no comparison between Berkovich indenter and conical indenter was made. However, this comparison was made in the examination stage of the proposed method which is the main purpose of the thesis.

Due to the axisymmetric geometry of conical indenter and cylindrical sample considered, analyses were made in two-dimension. Results of a nanoindentation test made on an elastoplastic aluminium alloy, Al 2024-T351, with 2000 nm penetration depth, was used [83]. An elastoplastic material was used to verify the numerical model, so that the verifications could be done without needing any rate-dependent parameters. Young's modulus, yield strength, and strain hardening exponent of the material were given in the paper as 68 GPa, 360 MPa, and 0.08, respectively. These material properties and poisson ratio of 0.40, for the sample, were input to the model, with mechanical properties of diamond having modulus of 1140 GPa and poisson ratio of 0.07. After making a comprehensive comparison taking the criteria given above into consideration, most convenient finite element model was selected for the further analyses.

4.2.1 Constitutive Model for the Elastoplastic Material

The sample material of the numerical model in the verification stage was modelled as isotropic hardening because the deformation to the material was made without reloading [84]. The material behaviour is determined with both an elastic and plastic component.

$$\boldsymbol{\varepsilon} = \boldsymbol{\varepsilon}^e + \boldsymbol{\varepsilon}^{pl} \quad (4.1)$$

where elastic component $\boldsymbol{\varepsilon}^e$ is defined as

$$\boldsymbol{\varepsilon}^e = \mathbf{S}\boldsymbol{\sigma} \quad (4.2)$$

where \mathbf{S} is the compliance matrix that is inverse of stiffness matrix and

$$\boldsymbol{\varepsilon}^p = \left(\frac{\boldsymbol{\sigma}}{K}\right)^{1/n} \quad (4.3)$$

Using the von Mises yield criterion, quadratic yield function is written as

$$f = \frac{3}{2}(\boldsymbol{\sigma}' - \boldsymbol{\alpha}):(\boldsymbol{\sigma}' - \boldsymbol{\alpha}) - \sigma_y^2 \leq 0, \quad (4.4)$$

where $\boldsymbol{\sigma}'$ and $\boldsymbol{\alpha}$ are the deviatoric part of the Cauchy stress tensor and back stress tensor, respectively, and σ_y is the initial yield stress. Since the material is modelled as isotropic hardening, back stress, $\boldsymbol{\alpha}$, becomes zero and deviatoric stress tensor.

$$\mathbf{s} = \boldsymbol{\sigma}' - \boldsymbol{\alpha} \quad (4.5)$$

becomes,

$$\mathbf{s} = \boldsymbol{\sigma}' \quad (4.6)$$

so that yield function has the form of

$$f = \frac{3}{2}(\boldsymbol{\sigma}'):(\boldsymbol{\sigma}') - \sigma_y^2 \leq 0 \quad (4.7)$$

where the yield stress

$$\dot{\sigma}_y = H \dot{\epsilon}^{pl} \quad (4.8)$$

$\dot{\epsilon}^{pl}$ is the rate of plastic flow and given as

$$\dot{\epsilon}^{pl} = \dot{\bar{\epsilon}}^{pl} \frac{\partial f(\boldsymbol{\sigma}')}{\partial(\boldsymbol{\sigma}')} \quad (4.9)$$

4.2.2 Determination of the Geometry of the Sample

In the first stage of the verification, quadratic quadrilateral plane elements with axisymmetry option were used. Also, tip roundness of 150 nm was taken into account. To meet the dimension of the roundness, additional mesh refinement at the contact region was applied. Nodes at the base of the sample model were fixed in all degrees of freedom. Symmetry boundary condition was applied through the nodes on the leftmost line of the model. Displacement boundary condition in the y direction was applied on top of the indenter. Node-to-surface contact was defined between the surfaces which will contact each other when boundary conditions are applied. The node number was about 5600.

Since the stress distribution occurred during the indentation process was not homogenous throughout the specimen, stress concentration was taken into consideration when meshing. In the region of indentation where stress is relatively higher, finer mesh was applied. Coarser mesh was gradually applied as depart from the indentation region to the edges of the specimen where stress level is very low. Due to the circular stress distribution during indentation, mesh graduation was made as to reflect the circular distribution of stress.

To decrease duration of the analyses and cost without compromising the accuracy of the analyses, smallest applicable specimen geometry with optimum node number is needed to be determined. Depending on the common decision in the literature [85], the thickness of the specimen was determined as 26000 nm which is approximately ten times of the maximum indentation depth made in the related experiments [86]. Although the tests, including the penetration depth of 1000 nm, was referenced for

the simulations, the value of 2600 nm was considered to make the model available for other tests reaching to the maximum penetration depth of 2550 nm.

After determining the thickness, width (or radius) of the specimen was calculated. Contrary to square geometry, which is commonly used for axisymmetric indentation simulations, width of the specimen was given a larger dimension compared to the thickness. When a model with square geometry (26000 nm × 26000 nm) is analysed, considerable displacement (26.5 nm or strain of 0.1) is observed at the upper edges of the specimen which is across the indentation region. That means, lateral stiffness of the specimen decreases with such geometry.

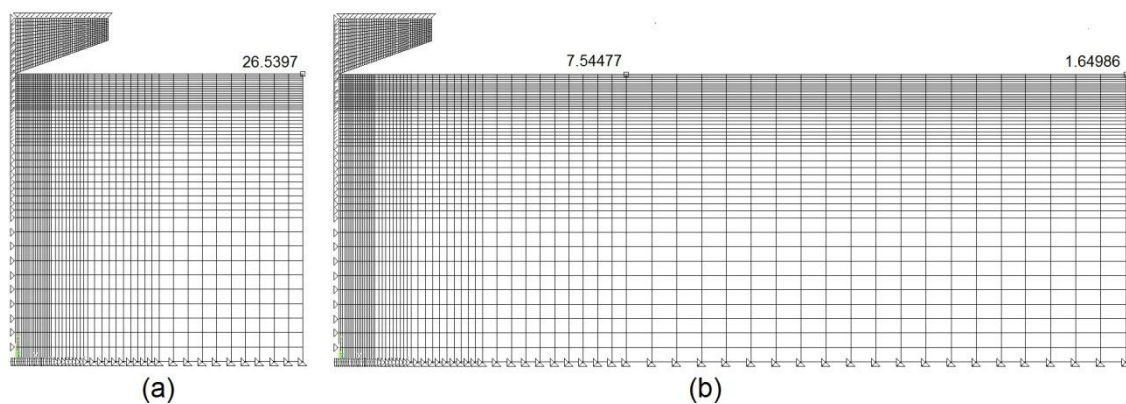


Figure 4.1 Specimen models; a) with square geometry, and b) with proposed geometry, shown with displacements on the edges

At the experiments, almost no displacement can occur at the edges of the specimen because indentation deformation is too small compared to the whole specimen volume. Depending on this argument the width of the specimen should be set as larger than the thickness of the specimen. For a determining factor, the angle of the specimen, which is 70.3 degree, was chosen. When calculated the tangent of the width of 26000 nm, the value of 72600 nm for the width is gained. After analysing the proposed model, the displacement of the node on the latter model, which is at the same location with the designated node on the square model, was found to be 3.5 times smaller (7.5 nm or strain of 0.029) than that of the designated node on the square model. Also the displacement at the edge was 1.65 nm. More importantly, the models with dimensions of 2600 nm × 7260 nm gave more approximate results than the models with dimensions of 26000 nm × 26000 nm did (see the graph below). For this reason, the proposed geometry was selected for further studies.

Although the load-displacement curve of the proposed model, compared to the square model, was closer to the experimental result, there were still distinctions between the results. The reason of the distinction of nose occurrence at the beginning of the unloading and the nonlinearity at the latest end of unloading was attributed to the rate-dependency of the material by the author of the paper. Also, there is slight difference between the loading curves. This difference can be attributed to the machining-induced stresses on the sample.

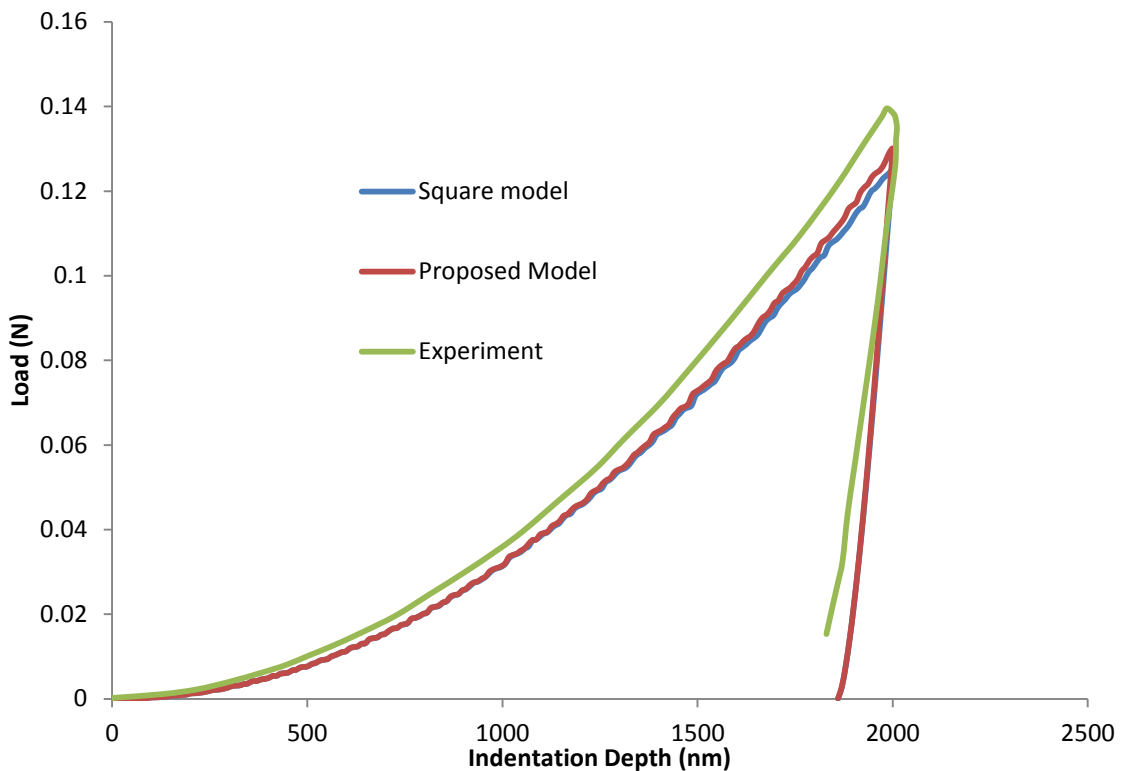


Figure 4.2 Comparison of experimental and numerical analysis results of nanoindentation on Al 2024-T351, from geometrical aspect

To see the effect of mesh density, models having different numbers of nodes were analysed. The model having 35000 nodes showed less accurate results although its path was much smooth. In contrast, model with 2000 nodes indicated a very wavy path while the maximum load was identical with that of the model having 5600 nodes (see Figure 4.3).

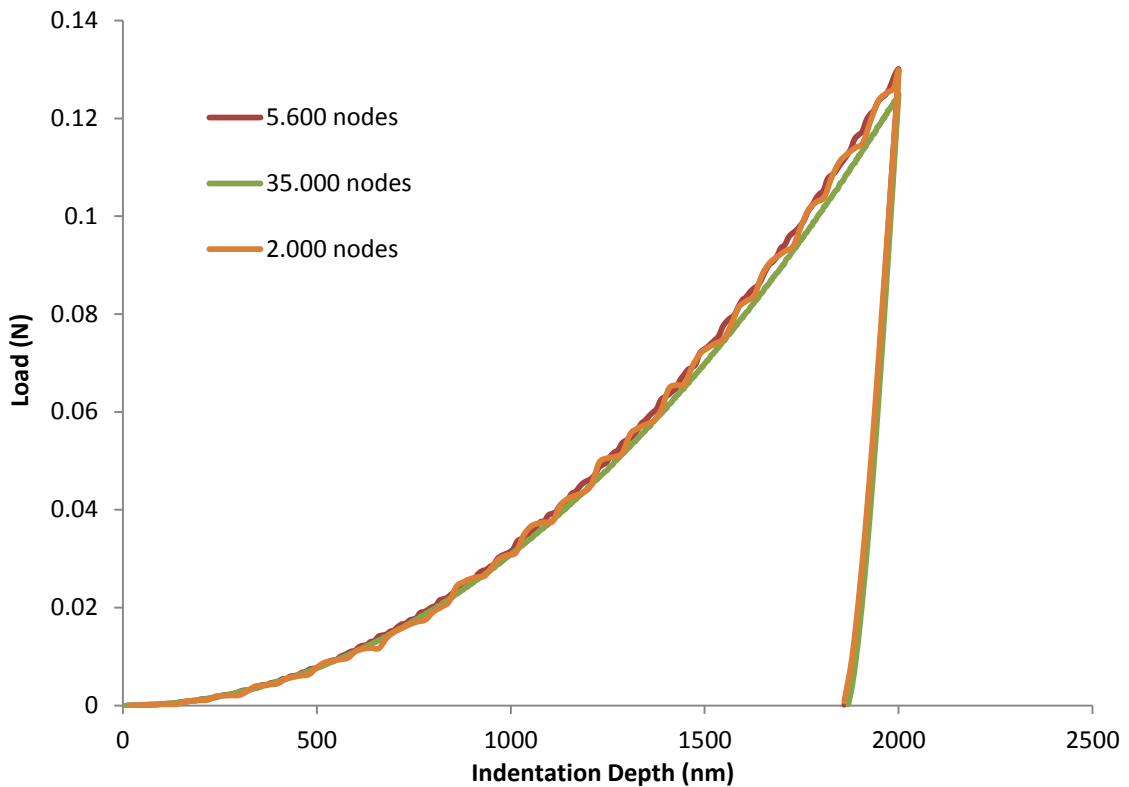


Figure 4.3 Comparison of the models in terms of node numbers, using the proposed model

4.2.3 Investigation of the Tip Bluntness Effect

In reality, none of the indenters have an ideal sharpness at their tips. Tip bluntness, or radius of curvature, may range between 40 nm and 150 nm. As they are used, they get blunter in time. Though, they may be modelled as perfectly sharp in finite element modelling if the resulting load-displacement curve does not deviate highly. Assumption of perfect tip is useful because analyses can be done using less numbers of elements with perfect tip. When tip roundness is taken into account, size of the elements are needed to be decreased, which results in more elements around contact region. Also, small elements with quadratic formulations led to errors of highly distortions, and analysis terminated. Element effect is also investigated under a different title.

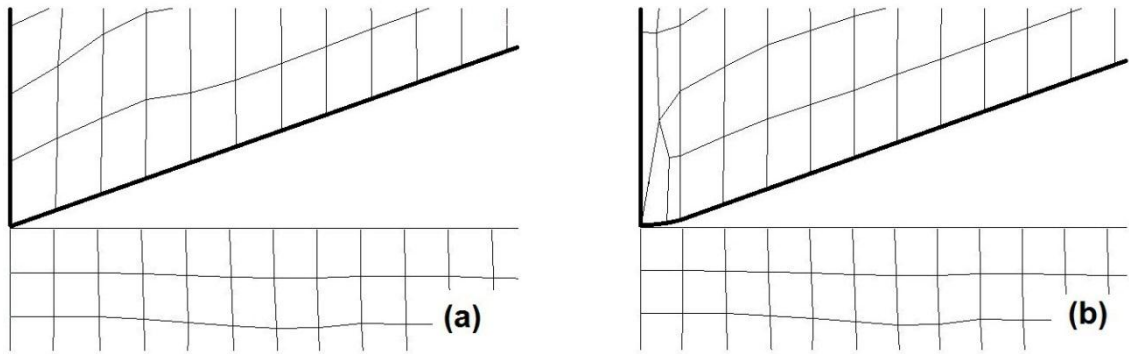


Figure 4.4 Indentation site showing the indenter: a) with sharp tip, and b) with blunt tip

A numerical model having perfect tip was modelled and compared with the one having a radius of curvature of 150 nm to see the tip bluntness effect. Elements were chosen as linear quadrilateral element because quadratic elements distort highly, leading to termination of the analysis, as mentioned before. Even though no mesh refinement was needed for perfect tip, refinement was applied to make a better comparison. Results showed that only 0.7 % difference occurred between the peak loads of two different models. Due to this, ideal tip assumption could be made.

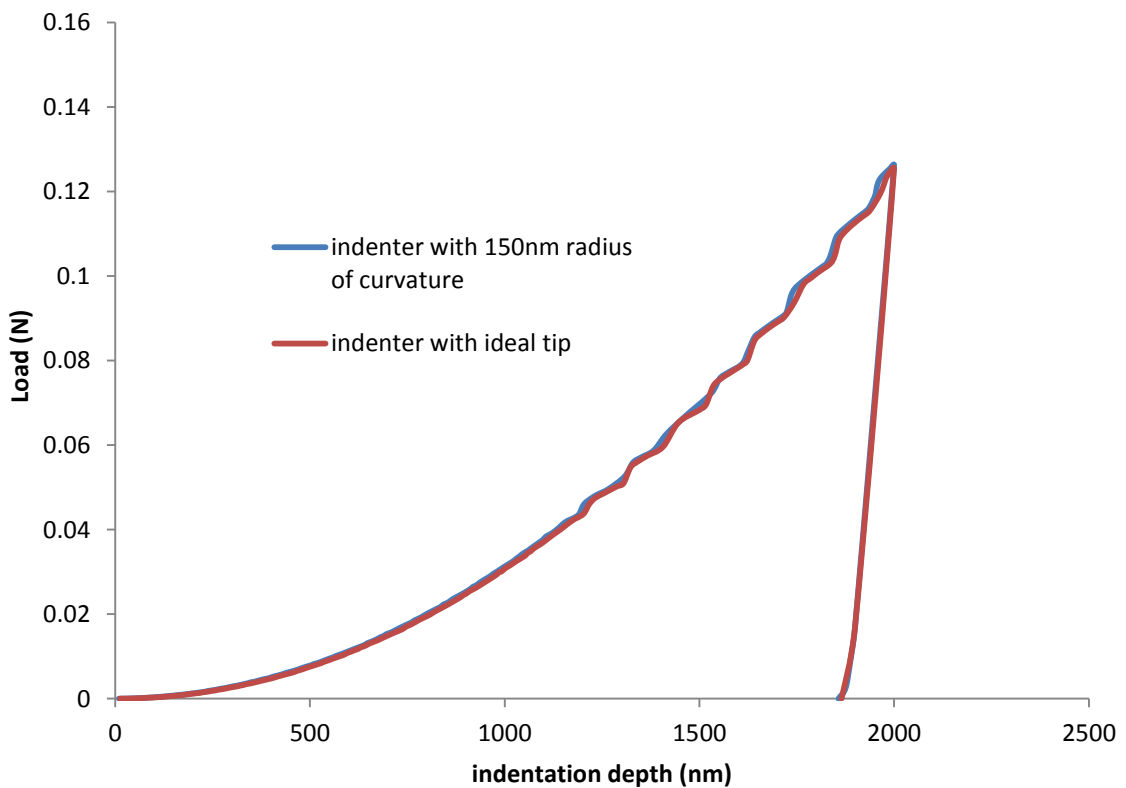


Figure 4.5 Comparison of the models in terms of tip roundness

4.2.4 Effect of Element Type

In the first two stages of verification, two different element types were used. One is linear and the other quadratic while both quadrilateral elements. Using quadratic element was generally assumed to give better result. But more time needed to solve an analysis involving quadratic elements.

Since the model used in this study two-dimensional, and not too much elements were used, the purpose of investigating element effect was due to the different element types used in the first two stages of the verification. If possible, quadratic elements would be used for the perfect tip having mesh refinement, and no element effect would be investigated. As it was stated before, quadratic elements do not work with additional mesh refinement in our model. Also, tips of the indenters were assumed as perfectly ideal. Therefore, no mesh refinement was applied in this stage of the verification. When compared the resulting load-displacement curves of the models, a difference between the peak loads, as small as 0.7 %, was observed. Also, the model with quadratic elements could predict nonlinearity at the latest ends of the unloading curve. For this reason, quadrilateral elements were applied for further studies.

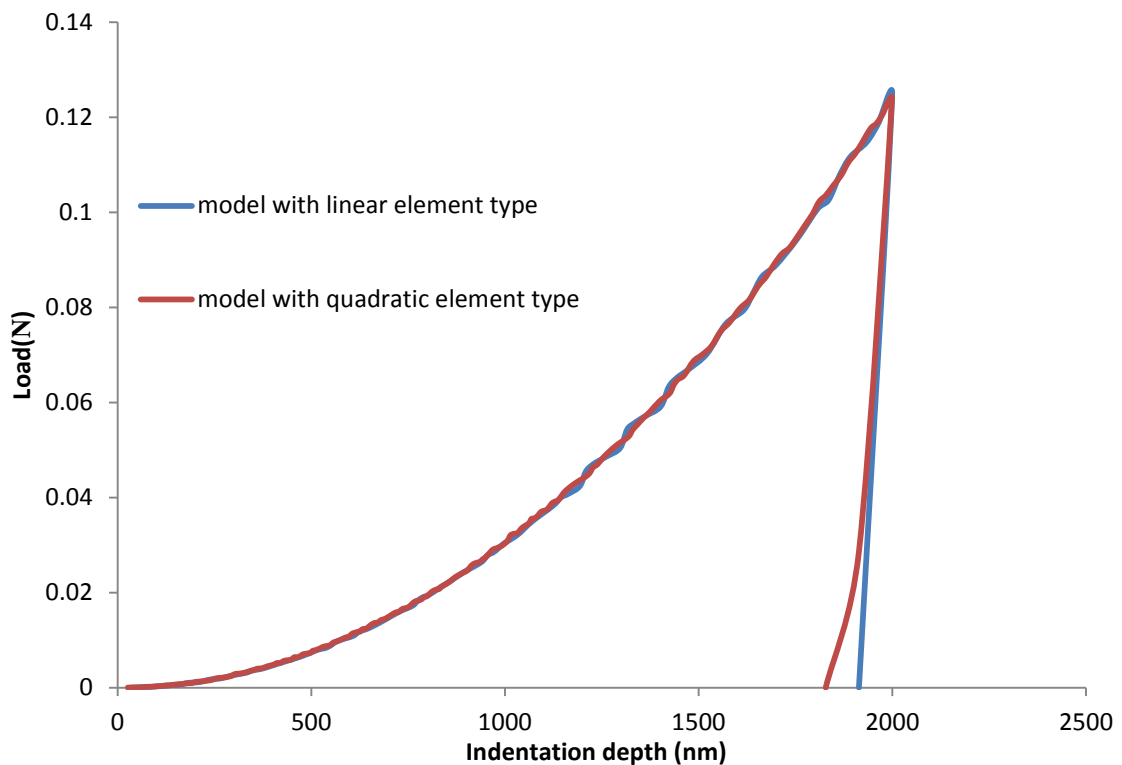


Figure 4.6 Comparison of the models in terms of element types

4.2.5 Effect of Mesh Refinement in the Contact Region

So far, the comparisons made included both the model with mesh refinement and the model without mesh refinement. Therefore, effect of mesh refinement on the analysis was thought to be useful. Perfect tip was selected and the mesh applied with linear elements because quadratic element did not work for the models including mesh refinement in the contact region. The difference between the resulting load-displacement curve was as small as to neglect it, i.e., peak load diverged with only 0.2 % error. For this reason, it was concluded that there is no need for mesh refinement in the contact region if the indenter was modelled as perfectly sharp.

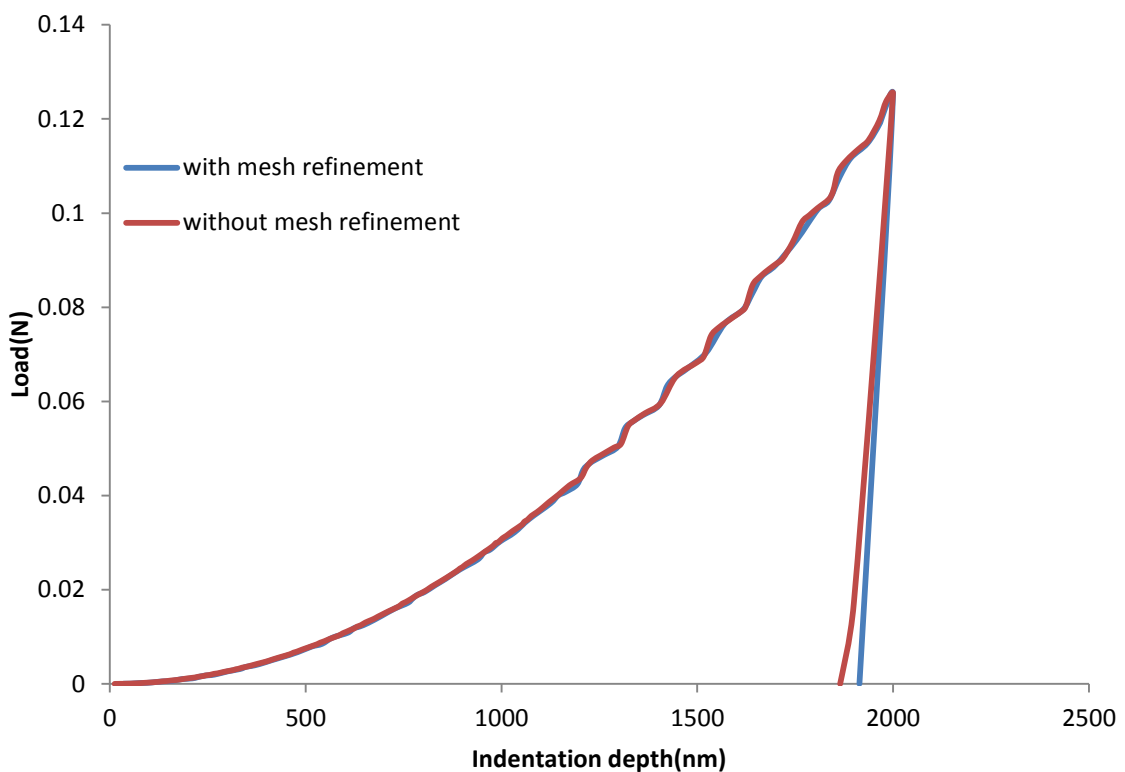


Figure 4.7 Comparison of the models in terms of mesh refinement around contact region

4.2.6 Conclusion on the Verification Stage

All the verification steps applied gave us a model which is easy to apply, can work fast, and is accurate enough. This model includes a sample geometry having dimensions, 2600 nm × 72600 nm, a perfectly sharp indenter with no mesh refinement, and quadratic element type. The determined model was used for further analyses in this study.

4.3 Viscoplastic Numerical Modelling of Nanoindentation

4.3.1 Experimental Work

Production of the pure epoxy sample and nanoindentation tests which are referenced in the thesis were conducted by Prof. Dr. Özgen Ü. ÇOLAK in Computational Nanomechanics Laboratory at Rensselaer Polytechnic Institute.

Load controlled and displacement controlled nanoindentations were made on epoxy sample using Hysitron Triboindenter®. To investigate the rate effect, the tests were performed at two different loading rates (200 nm/s and 20 nm/s for displacement controlled tests; 200 $\mu\text{N/s}$ and 20 $\mu\text{N/s}$ for load controlled tests). Also, cyclic loading were performed to see the softening or hardening behaviour of the material. Only load controlled experiments are of interest to this thesis (see Figure 4.8).

Load-displacement curves for epoxy were used to examine the method suggested, where viscoplastic material properties are obtained using nanoindentation tests and numerical analyses.

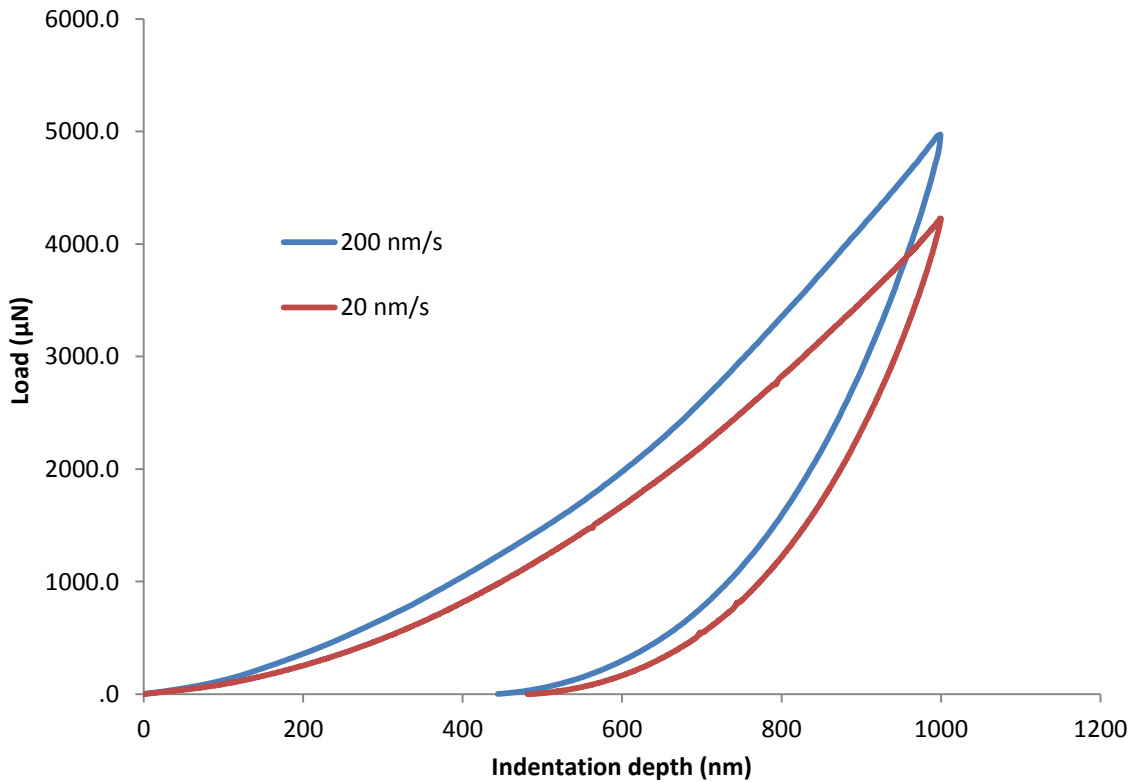


Figure 4.8 Load-displacement curves for pure epoxy (provided by Prof. Dr. Özgen Ü. ÇOLAK)

Production of 0.1 wt. % fraction GPL-epoxy nanocomposite and nanoindentation tests on the material, which were referenced in this thesis, were carried out by Ardavan ZANDIATASHBAR, Ph.D. candidate at Rensselaer Polytechnic Institute [87]. He performed the test in load control at a rate of 0.1 mN / s. The indentations were made on both close to and away from the protrusion sites where GPLs are relatively larger in number. With the aim of observing time-dependent behaviour of the material, he applied cyclic loading instead of monotonic loading. Although the numerical simulations we made for 0.1 wt. % of GPL-epoxy nanocomposite, which were done to make a comparison with the experiment, were not cyclic, the work of Zandiatashbar for the nanocomposite can still be referenced depending on his study on pure epoxy, where he applied and compared monotonic and cyclic nanoindentations, and reported that the curves were overlapping.

Since the filler fraction was very low and the indentations made was very shallow, the resulting load-displacement curves for each site, i.e., protrusion site and protrusion free site, were different from each other (see Figure 4.9). Although the material, in these tests, exhibited an anisotropic material behaviour, it is still isotropic, if manufactured properly, at bulk sizes. Therefore and for the sake of simplicity numerical model was built as isotropic.

In the reverse analysis, viscoplastic parameters were input as to provide that the resulting curve was between the two curves that are shown in Figure 4.9.

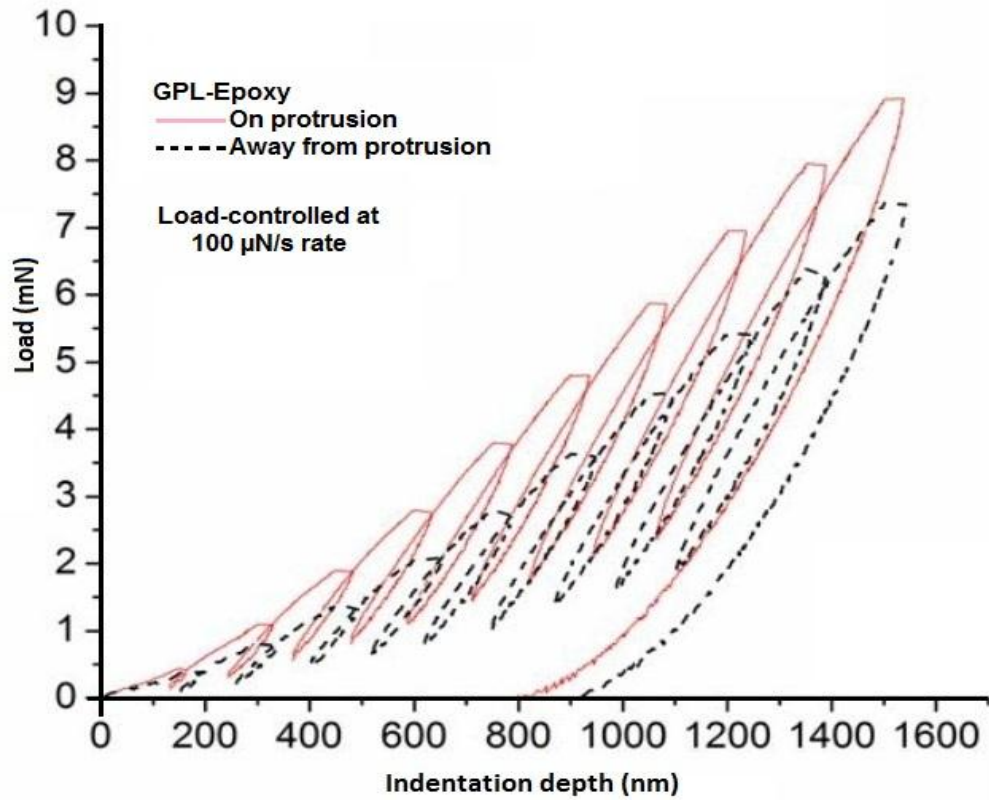


Figure 4.9 Load displacement curves for 0.1 wt. % fraction GPL-epoxy nanocomposite [87]

Tensile test for the same materials, were performed by Ardavan ZANDIATASHBAR at a rate of about 4.25×10^{-5} [65]. Resulting stress-strain curves were used to describe the material properties of the samples in the numerical models (see Figure 4.10).

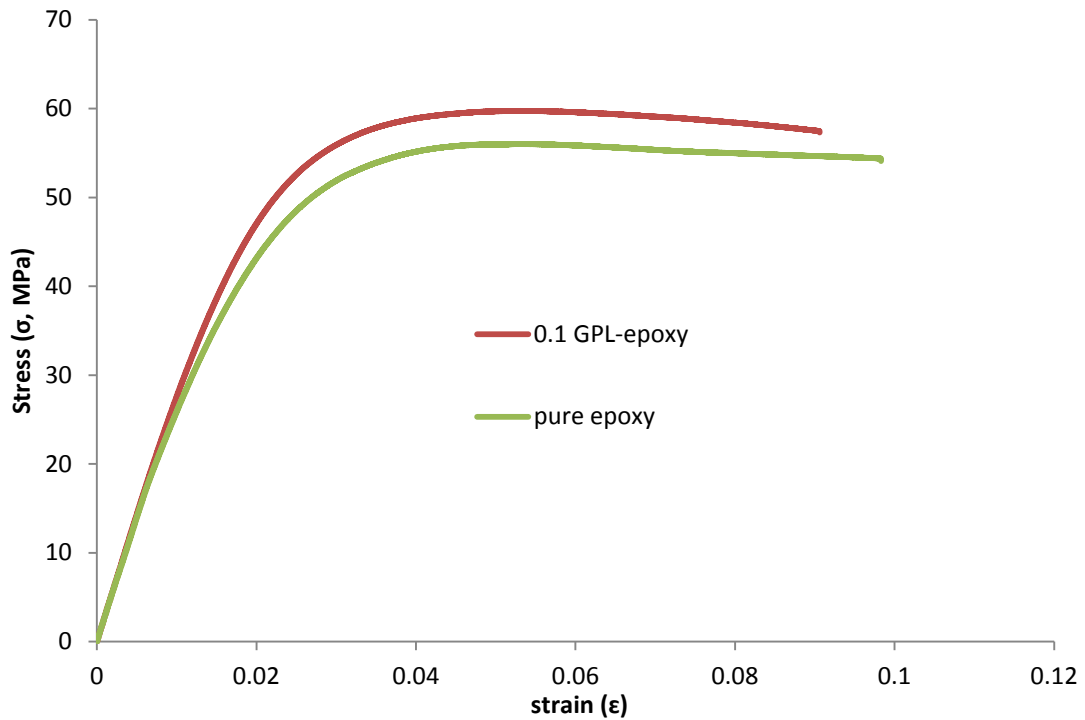


Figure 4.10 Stress-strain curves for pure epoxy and GPL-epoxy nanocomposites [85]

A forward analysis, obtaining nanoindentation behaviour of a material using tensile test data, was conducted to see the applicability of reverse analysis which was held under the next title. In the forward analysis, pure epoxy was used as sample material. Tensile test data for epoxy [85] was input to the analysis with a multi-linear form. Because ANSYS assumes yield point and proportional limit same, Young's modulus and yield strength were recalculated, according to the 0.2% offset rule, rather than using the values denoted. So, E for epoxy was determined as 2402.6 MPa and yield strength (or the first value for multi-linear curve) was calculated as 34.838 MPa. Also the softening part of the curve was neglected. The poisson ratio for pure epoxy was accepted as 0.4. Berkovich indenter was modelled as an elastic deformable body having a Young's modulus of 1140 GPa and poisson ratio of 0.07.

Existing viscoplastic material models in ANSYS are Perzyna, Peirce, Chaboche, and Anand. First two of them require fewer amounts of parameters. Therefore, they were examined for simulations.

In a viscoplastic analysis employing Perzyna or Peirce models, two material parameters, strain rate hardening exponent, m , and viscosity parameter, γ , are required to be incorporated to the model, which can be derived from tensile tests at

various rates. Therefore, tensile test data at different rates for a pure epoxy material was needed and the one reported by Zhoua et al. [88] was used (see Figure 4.11). Young's modulus of the epoxy they used is very close to the one used for defining the numerical model.

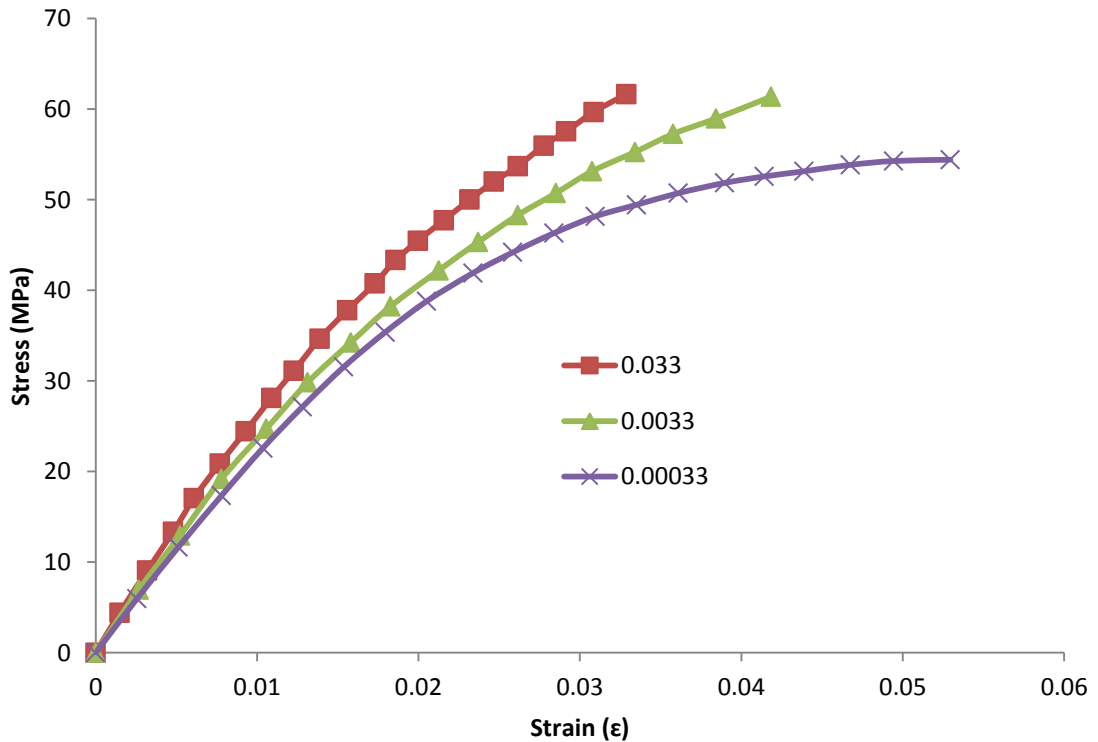


Figure 4.11 Stress-strain curves for pure epoxy at different loading rates [88]

In the nanoindentation analysis, elastic-viscoplastic material model was used for simplicity. Although there seems a small viscoelasticity at the stress-strain curves referenced, it was neglected in this study to find out viscoplastic parameters with a method explained by Avril et al. [89]. The material they used was not viscoelastic, while our material, epoxy, was slightly viscoelastic, the assumption of elastic behaviour for epoxy at different rates worked quite well. This argument was made by observing the resulting load-displacement curves for epoxy, which was obtained by changing the viscoplastic parameters and reanalysing the model, and comparing them with the test results provided by the thesis supervisor, Prof. Dr. Özgen Ü. Çolak.

4.3.2 Forward Analysis

4.3.2.1 Constitutive Model for the Elastoviscoplastic Material

As in the verification stage, the elastoviscoplastic materials, pure epoxy and GPL-epoxy nanocomposite was modelled as isotropic hardening. An elastoviscoplastic material has two strain components.

$$\dot{\boldsymbol{\varepsilon}} = \dot{\boldsymbol{\varepsilon}}^e + \dot{\boldsymbol{\varepsilon}}^{vp} \quad (4.10)$$

where elastic strain rate and viscoplastic strain rate are

$$\dot{\boldsymbol{\varepsilon}}^e = S\dot{\boldsymbol{\sigma}} \quad (4.11)$$

$$\dot{\boldsymbol{\varepsilon}}^{vp} = \gamma \left(\frac{\sigma}{\sigma_0} - 1 \right)^{1/m} \quad (4.12)$$

4.3.2.2 Determination of Viscoplastic Parameters of Pure Epoxy

Necessary parameters for both Perzyna and Peirce viscoplastic material models are strain rate hardening exponent, m , and viscosity parameter, γ .

The used viscoplasticity models, Perzyna and Peirce have the following form:

$$\dot{\boldsymbol{\varepsilon}}^{vp} = \gamma \left(\frac{\sigma}{\sigma_0} - 1 \right)^{1/m} \quad (4.13)$$

$$\dot{\boldsymbol{\varepsilon}}^{vp} = \gamma \left[\left(\frac{\sigma}{\sigma_0} \right)^{1/m} - 1 \right] \quad (4.14)$$

respectively, where σ_0 is the yield stress of the material at quasi-static tensile test, and σ is the material yield strength at a strain rate, $\dot{\boldsymbol{\varepsilon}}^{vp}$.

Although it was reported in the ANSYS manual that Peirce option gives better results, in this study Perzyna predicted nanoindentation behaviour better than Peirce.

The parameters m and γ were determined using the same method that Avril et al. applied [89]. In addition to their method, assumption of elastic behaviour substituting the viscoelastic behaviour for the epoxy was made. This was done by averaging the modulus of elasticity of the three stress-strain curves (see Figure 4.12).

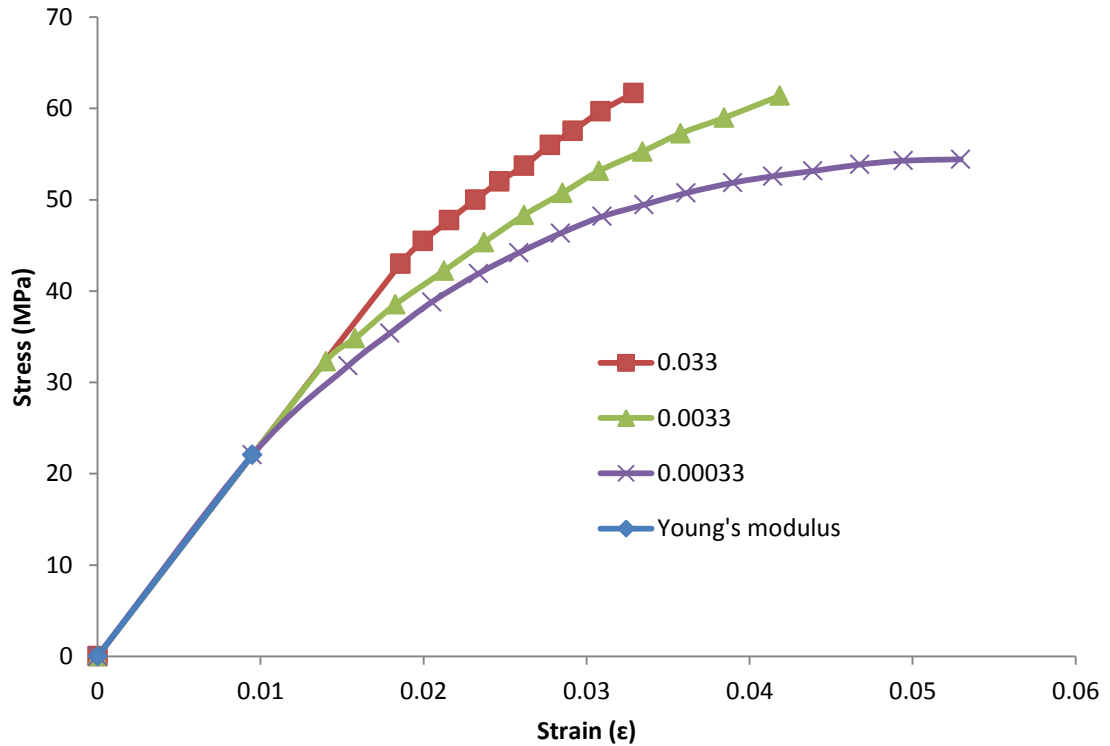


Figure 4.12 Tensile curves after neglecting the viscoelastic behaviour (for the original graph, see Figure 4.11)

Figure 19 is constructed using the following steps. First, a mean Young's modulus, 2402.6 MPa, is determined by averaging the E of each curve (those values are denoted in the related article [88]). This value also corresponds to the elastic modulus of the material that was tested at strain rate 0.0033. The value was offset to the point of 0.002 on the axis x and intersected with each curve, so that yield stress for each curve was determined (see Figure 4.12 and Table 4.1).

Table 4.1 Yield stresses, determined using 0.002 offset rule and applying common intersection, corresponding to each strain rate for pure epoxy

Strain rate (s ⁻¹)	0.033	0.0033	0.00033
Yield stress, σ (MPa)	44,64	32,29	21,27

Another parameter needed to determine the viscoplastic parameters from tensile data is the yield stress at quasi-static condition. This parameter was determined using the work of Miller et al. [90], where yield stress for pure epoxy was denoted as 17.7 MPa.

Avril et al. used a model derived by [91]:

$$\sigma = \sigma_0 + K_a(\dot{\epsilon}^{vp})^{1/n} \quad (4.15)$$

where K_a is named as stress rate sensitivity factor, n is strain rate sensitivity exponent.

Also,

$$K_a = \frac{\sigma_0}{\gamma^{1/n}} \quad (4.16)$$

Where γ was denoted as material viscosity parameter, and

$$\frac{1}{n} = m \quad (4.17)$$

which is strain rate hardening exponent.

Replacing the values in Figure 4.12 and value of σ_0 to equation (4.15), three equation combinations were gained;

$$44.64 = 17.7 + K_a(0.033)^{1/n} \quad (4.18)$$

$$32.29 = 17.7 + K_a(0.0033)^{1/n} \quad (4.19)$$

$$21.27 = 17.7 + K_a(0.00033)^{1/n} \quad (4.20)$$

Rearranging them,

$$26.94 = K_a(0.033)^{1/n} \quad (4.21)$$

$$14,59 = K_a(0.0033)^{1/n} \quad (4.22)$$

$$3.57 = K_a(0.00033)^{1/n} \quad (4.23)$$

so that three different equations with two unknowns were obtained. Although it seem that two equation is enough to get unknowns, for the most accurate determination of the unknowns each equations were equated to each other as to make three different combinations.

$$\frac{26.94}{(0.033)^{1/n}} = \frac{14,59}{(0.0033)^{1/n}} \quad (4.24)$$

$$\frac{26.94}{(0.033)^{1/n}} = \frac{3.57}{(0.00033)^{1/n}} \quad (4.25)$$

$$\frac{14,59}{(0.0033)^{1/n}} = \frac{3.57}{(0.00033)^{1/n}} \quad (4.26)$$

when these equations were solved, the values for n were found as 3.75, 1.64, and 2.28 from equations (4.18), (4.19), and (4.20), respectively. When calculated the average of these values, the value of 2.55 was found for n . Therefore, the strain rate hardening exponent

$$m = \frac{1}{2.55} = 0.3922 \quad (4.27)$$

was determined.

The other unknown, K_a , in equations (4.18), (4.19), and (4.20), was determined in the same way as the n determined. The value of n was substituted to the each equation combinations (equations (4.18), (4.19), and (4.20)) and K_{a1} , K_{a2} , and K_{a3} were found as 66.8, 481.7, and 120.51, respectively. When calculated the average of these values, the value of 223 was found for K_a . Inversing equation (4.16) and replacing the values found, viscosity parameter

$$\gamma = \left(\frac{\sigma_0}{K_a}\right)^n \quad (4.28)$$

$$\gamma = \left(\frac{17.7}{223}\right)^{2.55} \quad (4.29)$$

$$\gamma = 0.0016 \quad (4.30)$$

determined.

4.3.2.3 Numerical Simulations for Forward Analysis

Prior to starting the examination of forward analysis, applicability of the two-dimensional axisymmetric finite element model for the forward analysis, that was built as explained under the title numbered 4.2, was tested comparing the two-dimensional model and three dimensional model which includes Berkovich indenter.

As can be seen in Figure 4.13a, the sample in the three-dimensional model was generated by sweeping the previously generated and selected two-dimensional finite element model. Berkovich indenter model was built on the swept model (see Figure 4.13b). Mesh pattern at the contact region of the Berkovich indenter was applied as to correspond to the mesh pattern at the contact region of the sample model (see Figure 4.14).

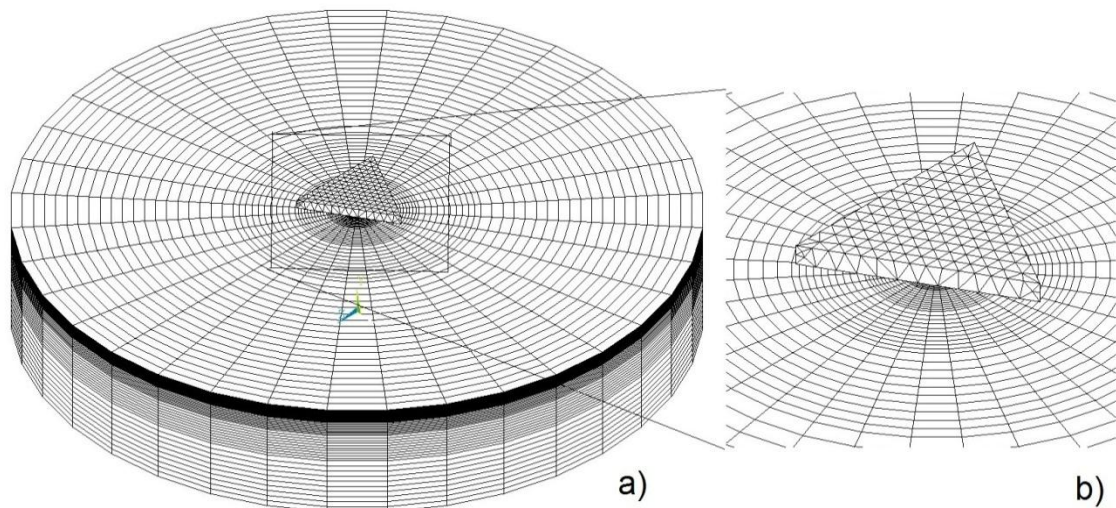


Figure 4.13 Finite element model of a Berkovich indentation: a) Volume of the sample, which is generated by sweeping the 2-D sample model. b) Detailed image of Berkovich indenter on the sample

Perzyna option was chosen for the simulations and parameters were taken from the study given under the previous title. Mechanical properties of pure epoxy is as in Figure 4.10. Material of indenters were determined as deformable diamond.

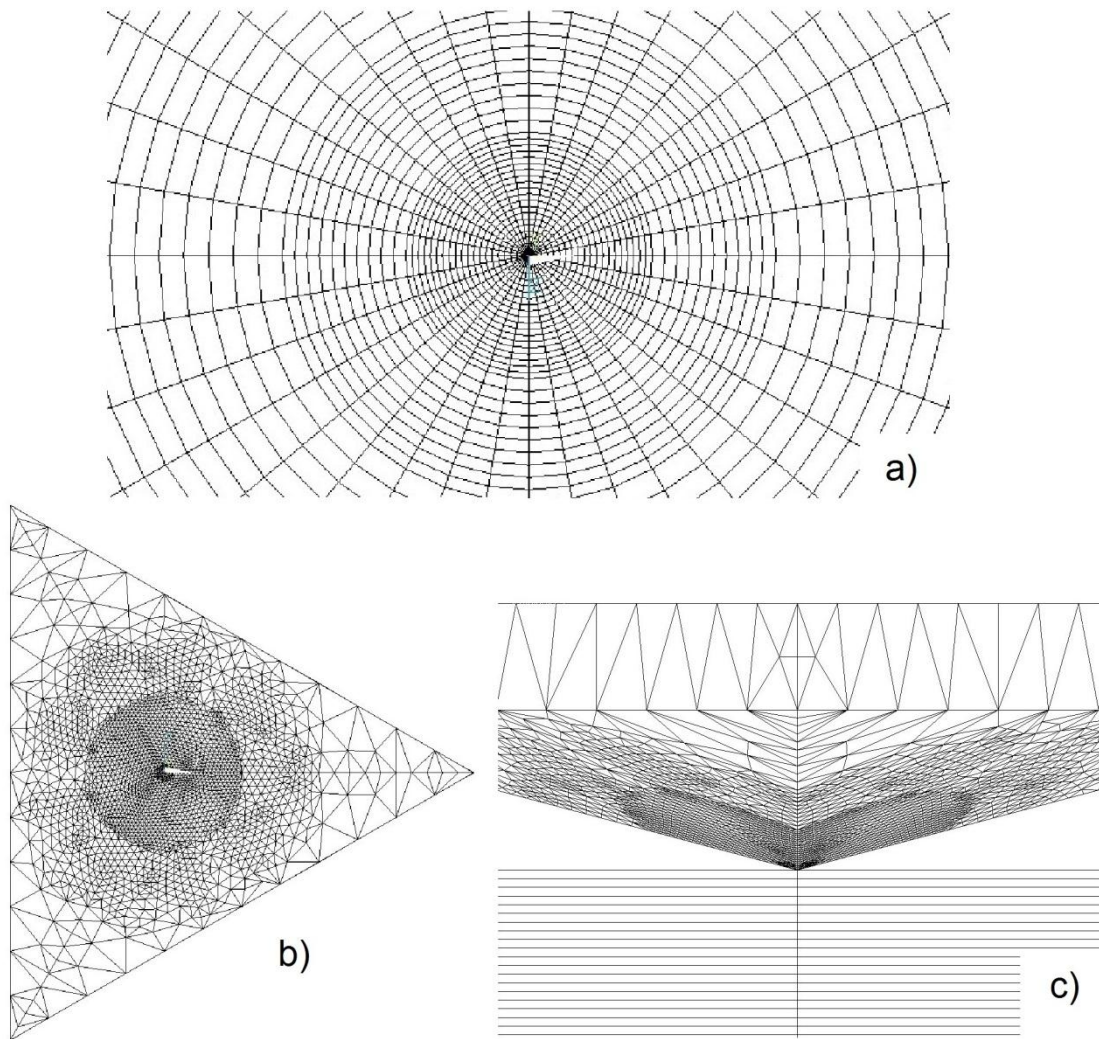


Figure 4.14 Mesh pattern of Berkovich indentation: a) Top of the sample that is around the indentation site; b) Bottom of the Berkovich tip, showing the similar element distribution to the one on the sample; c) Element distribution on the Berkovich indenter (from a different point of view)

To keep the analysis duration short, linear 3-D elements, hexahedral for the sample model and tetrahedral for the indenter model, were used in three-dimensional model. In this case, for an accurate comparison, linear quadrilateral elements were preferred for two-dimensional model.

For both models, bottom of the sample was fixed in all directions while a predetermined displacement in the y direction was applied on the top of the indenter. Also, for 3-D model, the top of the indenter was fixed in the x and z direction to provide a stable boundary condition for the indenter. For both models, frictionless

node-to-surface contact was defined between the surfaces where the contact will occur when boundary conditions are applied.

Load-displacement (P-h) curves of the analyses were obtained as shown in Figure 4.15. In contrast to the expected result, P-h curve of the 3-D model is a bit different than the experimental value. There are several reasons for that result. Some of them geometry and material effect, local stresses and strains etc. [92]. Evaluation of such reasons is not in the scope of the current study. Also, the time required to solve a 3-D analysis is 120 times more than that for a 2-D analysis. Moreover, the desired results are obtained using conical (2-D) indentation analysis as can be seen in Figure 4.20 and Figure 4.21. Therefore conical indentation was chosen instead of Berkovich indentation.

Von Mises stress distributions and total displacements at peak loads can be seen in Figure 4.16, and Figure 4.17. As can be seen from the figures, sink-in occurred in both indentations because E/σ_y value is low for pure epoxy, suggesting that it is hard material.

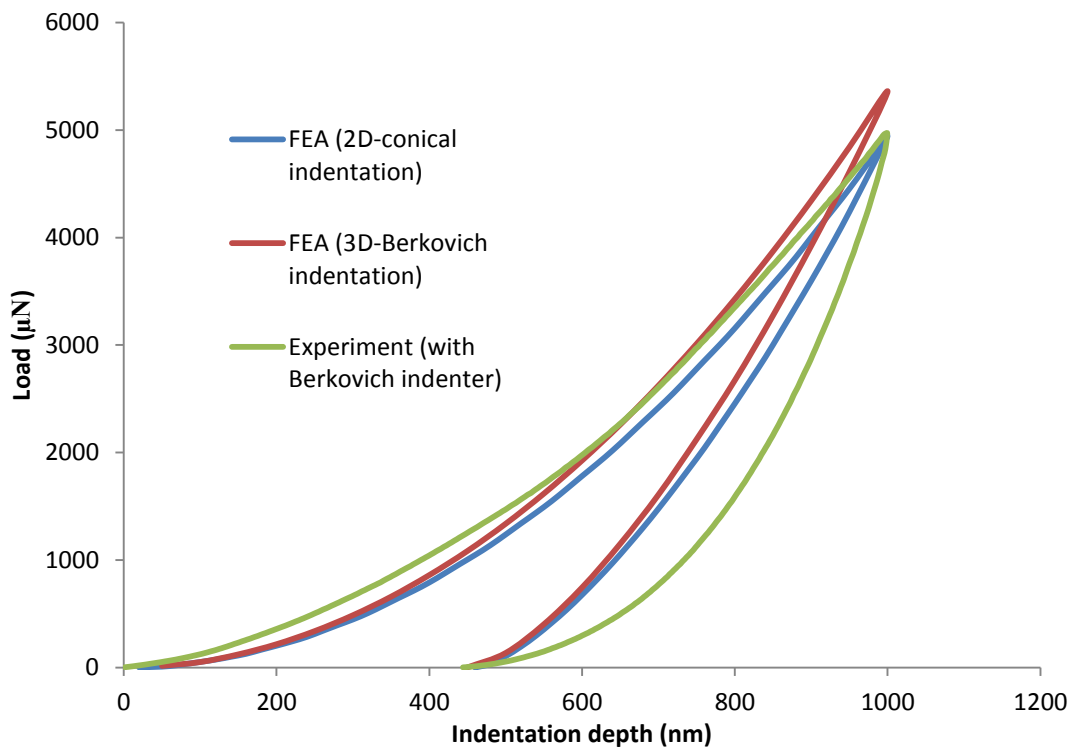


Figure 4.15 Comparison of load-displacement curves of conical, Berkovich nanoindentation simulations and experiment at a displacement rate of 200 nm/s on pure epoxy

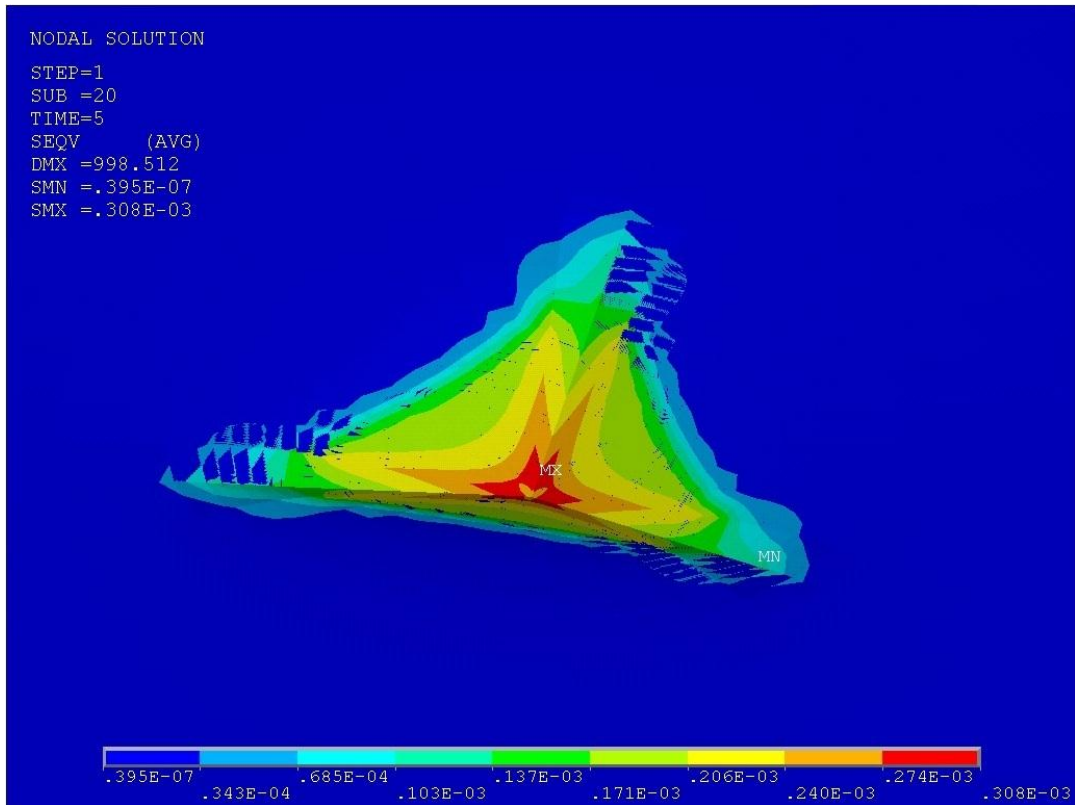


Figure 4.16 Von Mises stress distribution around indentation site on pure epoxy sample, at peak load, for Berkovich indentation

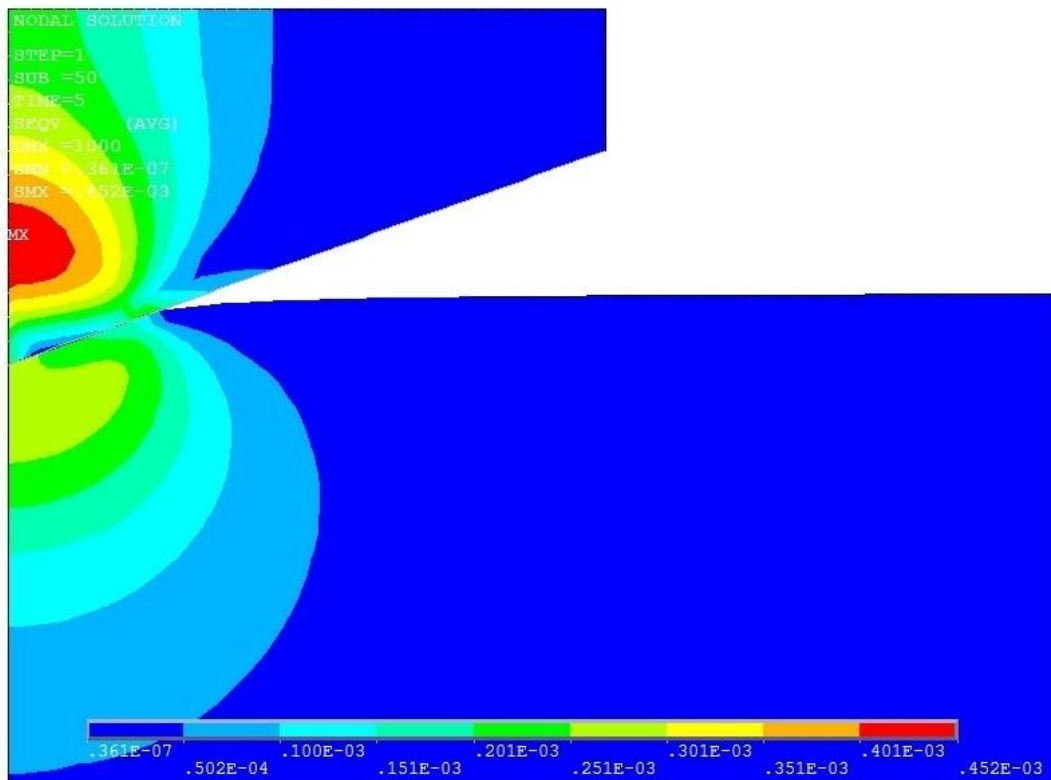


Figure 4.17 Von Mises stress distribution around indentation site on pure epoxy sample, at peak load, for conical indentation

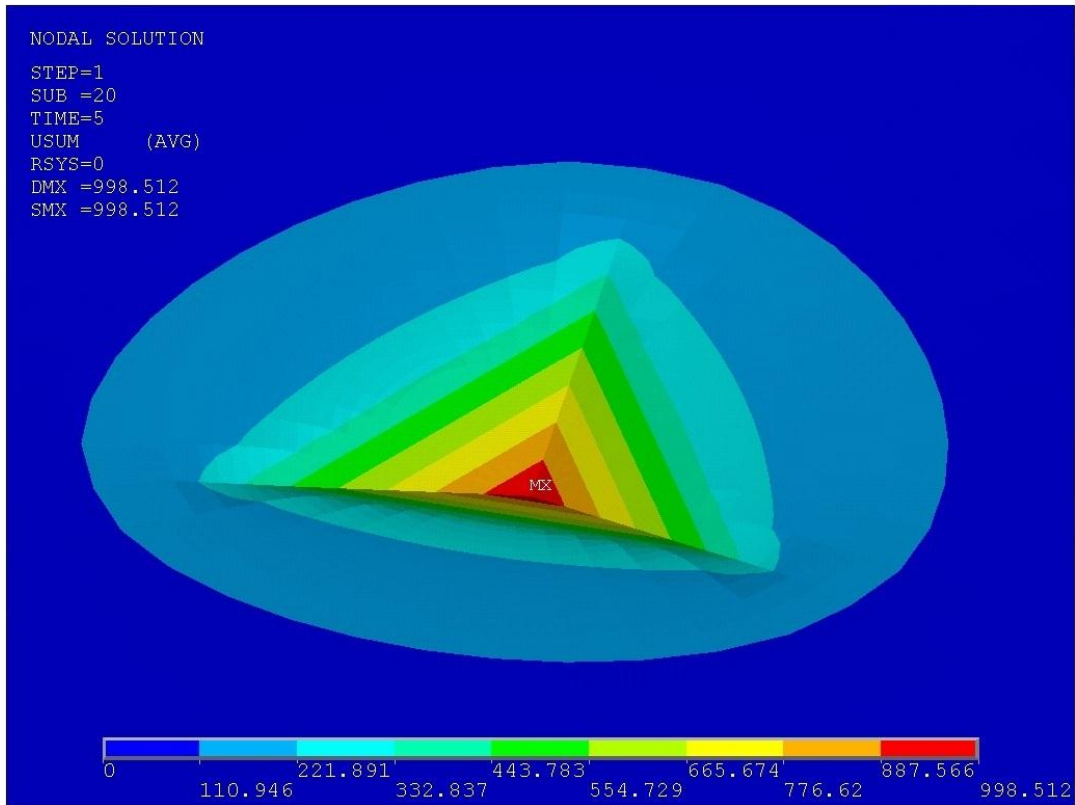


Figure 4.18 Contour of total displacement around indentation site on pure epoxy sample, at peak load, for Berkovich indentation

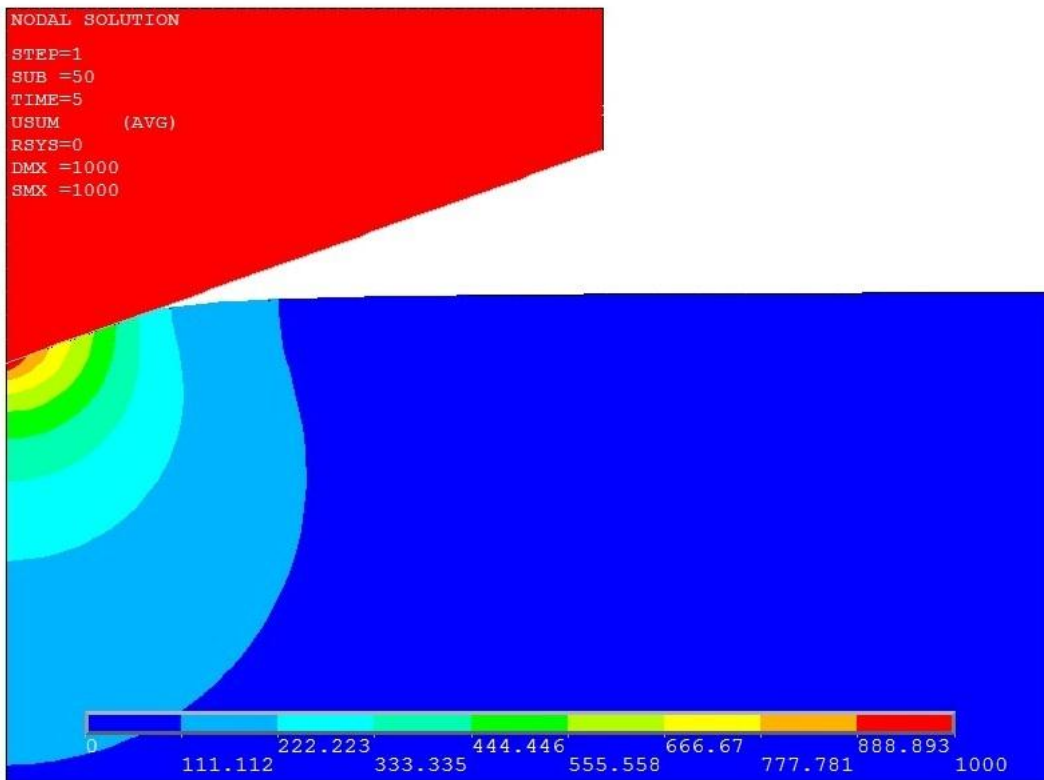


Figure 4.19 Contour of total displacement around indentation site on pure epoxy sample, at peak load, for conical indentation

So far, all the parameters were determined. At this stage, the parameters were input to the analysis with both Perzyna option and Peirce option at two different displacement rates. Resulting curves showed that Peirce could predict nonlinearity in unloading better than Perzyna while Perzyna could almost exactly predicted the peak load compared to misestimation of Peirce (see Figure 4.20 and Figure 4.21).

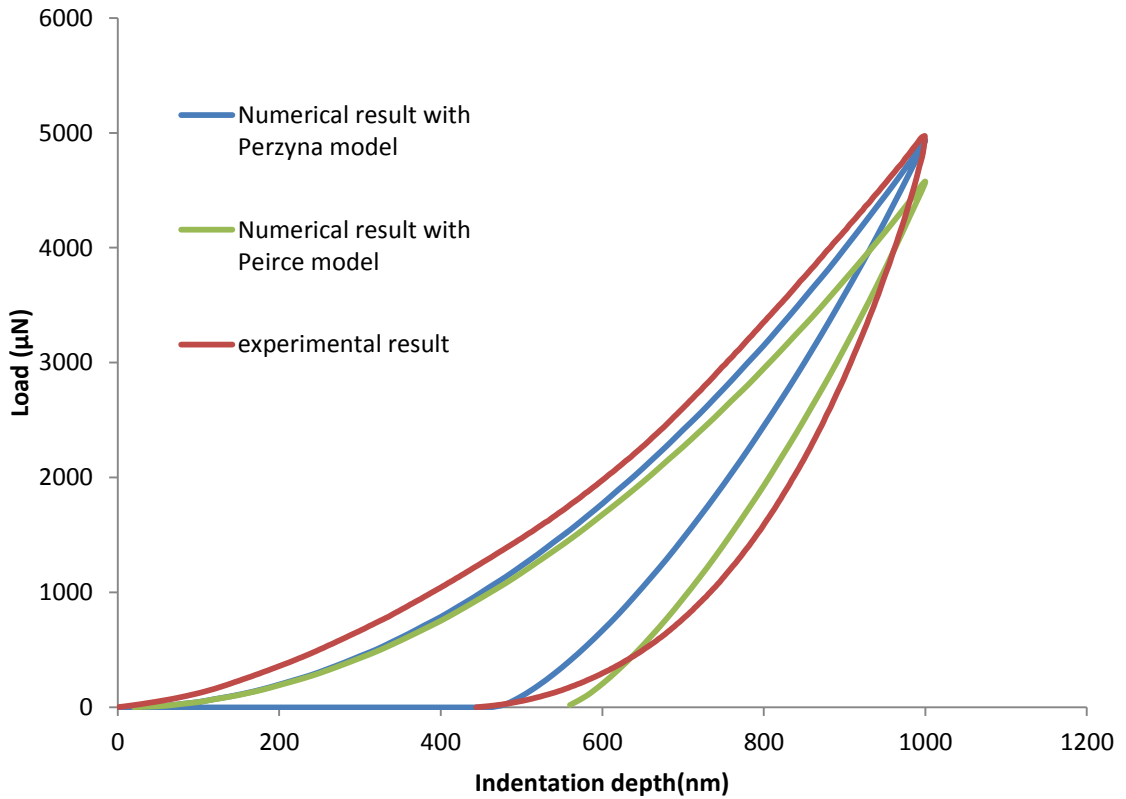


Figure 4.20 Comparison of the load displacement curves of the numerical models and experiment on pure epoxy at displacement rate of 200 nm/s

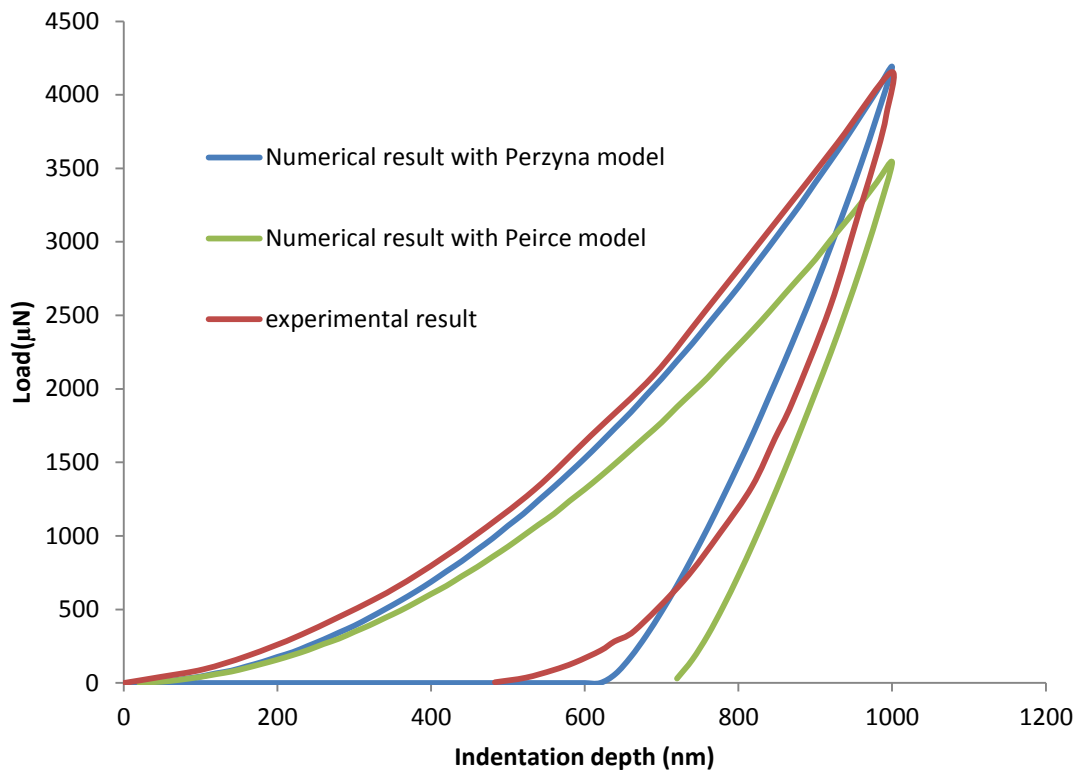


Figure 4.21 Comparison of the load displacement curves of the numerical models and experiment on pure epoxy at displacement rate of 20 nm/s

4.3.2.4 Conclusion on the Forward Analysis

Numerical results showed that Perzyna and Peirce viscoplastic material models cannot converge properly the mechanical behaviour of a material under nanoindentation deformation. Though, the Perzyna model could estimate very well the peak load for both displacement rates. Therefore, it was concluded that the Perzyna model can be used for reverse analysis where viscoplastic parameters are determined using the numerical analyses of nanoindentation in accordance with experimental nanoindentation data.

4.3.3 Reverse Analysis

It was understood from the forward analysis that viscoplastic properties of a material can be obtained from a process which includes a quasi-static tensile test, nanoindentation test at only one rate (more than one rate is proper as well), and a finite element modelling of nanoindentation that employs Perzyna viscoplastic material model and has the same boundary conditions with related nanoindentation

test. In the first step, a quasi-static tensile test and a nanoindentation test of a material are performed. Second step is to build a verified numerical model and to input the material property data obtained from quasi-static tensile test. In the last step viscoplastic parameters are arbitrarily input as such the resulting load-displacement curve converge the experimental curve at peak load. When the analysis result converge the experimental result at the peak load of load-displacement curve, the arbitrarily input parameters are accepted as the viscoplastic parameter of the related material.

The experiment was conducted at load controlled mode using the rate of $100 \mu\text{N/s}$ in accordance with displacement limit controls [87]. To simulate the conditions of the experiment better, displacement controlled analyses were conducted by calculating the average testing time. It was computed as 164 seconds with maximum displacement of 1500 nm.

The material of interest, 0.1 wt. % fraction GPL-epoxy, is not homogeneous at certain length-scales. Therefore, the experimental data referenced for 0.1 wt. % fraction GPL-epoxy has two load displacement curves indicating the two different phase of the material. Following the steps given above, a number of analyses were performed and the resulting curve was attempted to be provided between the two experimental curves of the material.

Since the parameters to be determined are more than one, a table showing the effect of two parameters was prepared (see Table 4.2). Experimental and numerical analysis results are depicted together in Figure 4.22 to show that the curves of the simulations, which are between the experimental curves, have the approximate viscoplastic parameters, γ and m , suggesting that they are possible viscoplastic parameters for 0.1 wt. % fraction GPL-epoxy nanocomposite. A small drawback here is that none of the curves gained from numerical analyses are exactly between the experimental curves. This is because the experiment in hand is load controlled, while the simulations are displacement controlled. Though, since peak loads are of interest, the curves, of which the peak loads are between the peak loads of experimental curves, are accepted as they are between the experimental curves providing that they achieved to simulate the real tests approximately. It can be concluded that the strain rate hardening

exponent m and viscosity γ of the material ranges between 0.3-0.5, and 0.1-0.01, respectively.

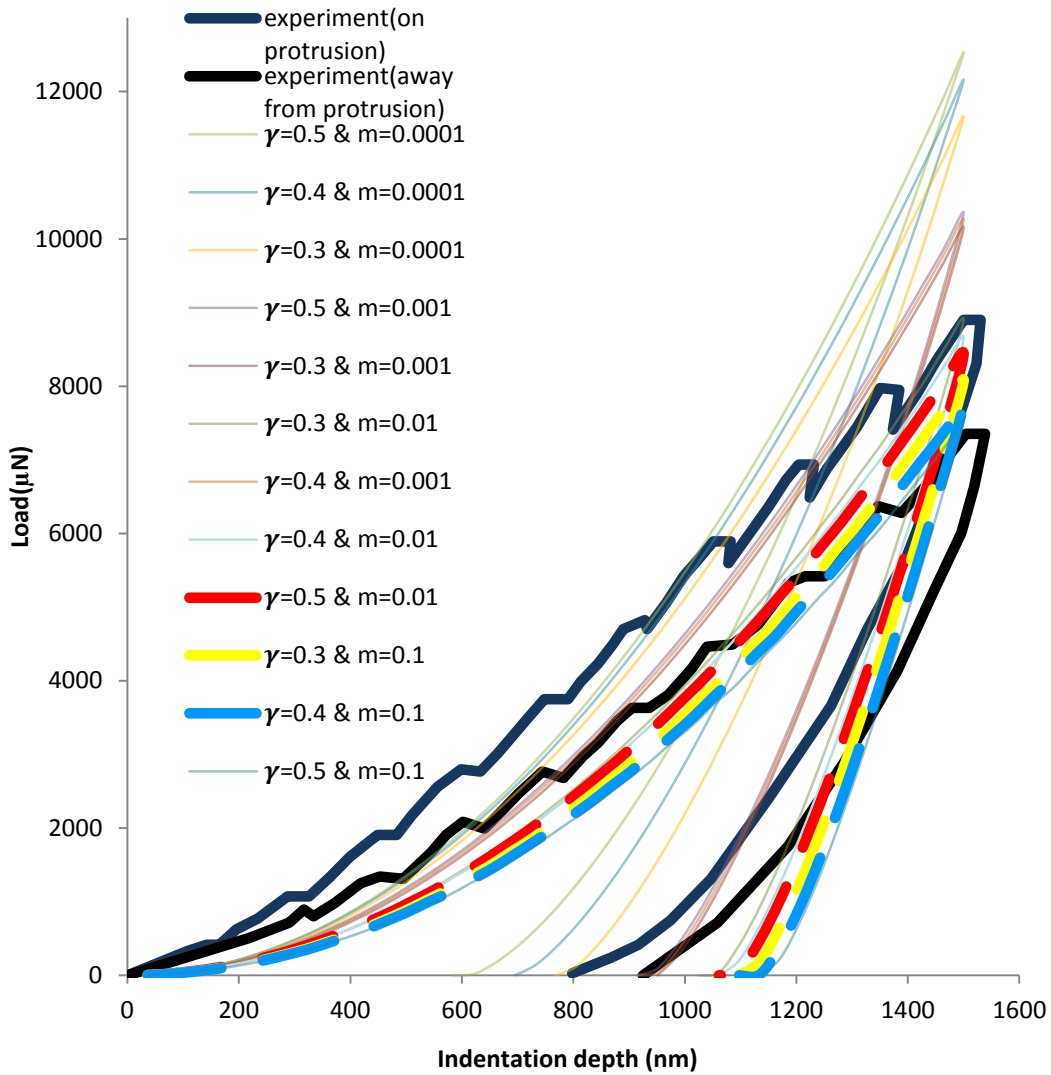


Figure 4.22 Comparison of the load-displacement curves of experiments [87] and numerical models that were given various viscoplastic parameters, which were conducted for 0.1 wt. % fraction GPL-epoxy (The curves having thick and dashed lines are those providing approximate m and γ values. The experimental curves are modified to make the graph clearer, see Figure 4.9 for the original curves)

Table 4.2 Peak load values (in Newton) obtained from the simulations (blue coloured values indicate that they are between the experimental values)

γ \ m	0.3	0.4	0.5
0.0001	11663	12161	12532
0.001	10158	10264	10356
0.01	8912	8664	8441
0.1	8065	7756	7527

RESULTS AND DISCUSSION

In this study, the identification of viscoplastic material properties of a graphene-epoxy nanocomposite using tests and numerical models of nanoindentation were researched.

Graphene-epoxy nanocomposites and nanoindentation process were studied. Advantages of graphene over other nano materials, production of graphene and graphene epoxy nanocomposite were explained. Theory of nanoindentation was studied based on the works, in literature, carried out so far.

This study mainly aimed to examine the applicability of nanoindentation process as viscoplastic material characterisation method. Analyses and experiments showed that the method is applicable for nanocomposite materials to some extent. But for completely homogeneous isotropic materials, the method can easily be applied. For the ease of application of the method for nanocomposites, homogenisation techniques can be applied.

In the verification stage, some findings have been gained such as an effective geometric model for sample of indentation. Analyses showed that the proposed geometry gives better results than conventional square geometry. Since the used material, Al 2024-T351, is appropriate for the assumption of conical indentation equivalency, no comparison between Berkovich (3-D) and conical (2-D) indentation was made.

The aim of the forward analysis, was to examine the proposed method. Before doing examination, three-dimensional numerical nanoindentation analysis was carried out to see the equivalency of two-dimensional models for the epoxy and epoxy based nanocomposite material. Load-displacement curve of the 3-D analysis was slightly different than the experimental values while 2-D analysis has shown much closer results to the experiments. In the literature, the reasons for such cases are explained and some correction factors were applied to fix the results. Since the 2-D model gave the expected results, it was used for forward and reverse analyses.

In the forward analysis, viscoplastic material parameters were determined analytically and put into the numerical models with both Perzyna and Peirce viscoplastic material models. The analyses were conducted at two different displacement rates as in the experiments. Results showed that Perzyna model can predict material behaviour much accurately compared to Peirce model. Therefore, Perzyna model was decided to be used for reverse analysis.

In the reverse analysis, stress-strain curve [65] of 0.1 wt. % fraction GPL-epoxy nanocomposite was input to the finite element model. Result of a nanoindentation test on the same material [87], which are load controlled and conducted at a rate of $100 \mu\text{N/s}$, was used as a reference to numerical simulations. Arbitrarily chosen values for m and γ were input to the numerical model and simulations were carried out for each input. The parameters, which provide a close load-displacement curve, were accepted as viscoplastic material parameters for 0.1 wt. % fraction GPL-epoxy nanocomposite.

Depending on the forward analysis, it can be stated that, given a much homogenous material, the parameters could be determined with a greater accuracy. This study can be further developed by applying homogenisation techniques and incorporating optimisation algorithms into the method.

REFERENCES

- [1] Coleman, J. N., Khan, U., Blau, W. J., and Gun'ko, Y. K., (2006). "Small but strong: A review of the mechanical properties of carbon nanotube-polymer composites", *Carbon*, 44 (9): 1624-1652.
- [2] Park, S., An, J. H., Piner, R. D., Jung, I., Yang, D. X., Velamakanni, A., Nguyen, S. T., and Ruoff, R. S., (2008). "Aqueous Suspension and Characterization of Chemically Modified Graphene Sheets", *Chemistry of Materials*, 20 (21): 6592-6594.
- [3] Bai, H., Xu, Y. X., Zhao, L., Li, C., and Shi, G. Q., (2009). "Non-covalent functionalization of graphene sheets by sulfonated polyaniline", *Chemical Communications*,(13): 1667-1669.
- [4] Hu, H., Onyebueke, L., and Abatan, A., (2010). "Characterizing and modeling mechanical properties of nanocomposites-review and evaluation", *Journal of Minerals & Materials Characterization & Engineering*, 9 (4): 275-319.
- [5] Iijima, S., (1991). "Helical microtubes of graphitic carbon", *Nature*,(354): 56-58.
- [6] Wallace, P., (1947). "The band theory of graphite", *Physical Review*, 71: 622-634.
- [7] Novoselov, K. S., Geim, A. K., Morozov, S. V., Jiang, D., Zhang, Y., Dubonos, S. V., Grigorieva, I. V., and Firsov, A. A., (2004). "Electric field effect in atomically thin carbon films", *Science*, 306 (5696): 666-669.
- [8] Rafiee, M. A., Rafiee, J., Wang, Z., Song, H. H., Yu, Z. Z., and Koratkar, N., (2009). "Enhanced Mechanical Properties of Nanocomposites at Low Graphene Content", *Acs Nano*, 3 (12): 3884-3890.
- [9] Park, S., and Ruoff, R. S., (2009). "Chemical methods for the production of graphenes", *Nature Nanotechnology*, 4 (4): 217-224.
- [10] McAllister, M. J., Li, J. L., Adamson, D. H., Schniepp, H. C., Abdala, A. A., Liu, J., Herrera-Alonso, M., Milius, D. L., Car, R., Prud'homme, R. K., and Aksay, I. A., (2007). "Single sheet functionalized graphene by oxidation and thermal expansion of graphite", *Chemistry of Materials*, 19 (18): 4396-4404.

- [11] Wahlberg, A., (1901). "Brinell's method of determining hardness and other properties of iron and steel", *Journal of the iron and steel institute*, 59: 243.
- [12] Meyer, E., (1908). "Investigations of hardness testing and hardness", *Phys. Z.*, 9: 66.
- [13] Rockwell, S. P., (1922). "The testing of metals for hardness", *Transactions of the American Society for Steel Treating*, 2: 1013.
- [14] Smith, R., and Sandland, G., (1922). "An accurate method of determining the hardness of metals, with particular reference to those of a high degree of hardness", *Proceedings of the Institution of Mechanical Engineers*, 1: 623.
- [15] Tabor, D., (1948). "A simple theory of static and dynamic hardness", *Proceedings of the Royal Society-A*, 192: 247.
- [16] Hertz, H., (1881). "On the contact of elastic solids", *The Journal für die reine und angewandte Mathematik*: 156-171.
- [17] Bishop, R. F., Hill, R., and Mott, N. F., (1945). "The theory of indentation and hardness tests", *Proceedings of the Physical Society*, 57: 147.
- [18] Hill, R., Lee, E. H., and Tupper, S. J., (1947). "The theory of wedge indentation of ductile materials", *Proceedings of the Royal Society-A*, 188: 273.
- [19] Hill, R. (1950). *The Mathematical Theory of Plasticity*. Clarendon Press, Oxford.
- [20] Tabor, D., (1996). "Indentation hardness: Fifty years on a personal view", *Philosophical Magazine A*, 74 (5): 1207 — 1212.
- [21] Pethica, J. B., Hutchings, R., and Oliver, W. C., (1983). "Hardness Measurement at Penetration Depths as Small as 20-Nm", *Philosophical Magazine a-Physics of Condensed Matter Structure Defects and Mechanical Properties*, 48 (4): 593-606.
- [22] Bulychov, S. I., and Alekhin, V. P., (1987). "Method of Kinetic Hardness and Microhardness in Testing Impression by an Indentor", *Industrial Laboratory*, 53 (11): 1091-1096.
- [23] Doerner, M. F., and Nix, W. D., (1986). "A method for interpreting the data from depth-sensing indentation instruments", *Journal of Materials Research*, 1: 601-609.
- [24] Sneddon, I. N., (1965). "The relation between load and penetration in the axisymmetric Boussinesq problem for a punch of arbitrary profile", *International Journal of Engineering Science*, 3: 47-57.
- [25] Berkovich, E. S., (1950). "Three-Faceted Diamond Pyramid for Studying Microhardness by Indentation", 13: 45-347.
- [26] Oliver, W. C., and Pharr, G. M., (1992). "An Improved Technique for Determining Hardness and Elastic-Modulus Using Load and Displacement Sensing Indentation Experiments", *Journal of Materials Research*, 7 (6): 1564-1583.

- [27] Jayaraman, S., Hahn, G. T., Oliver, W. C., Rubin, C. A., and Bastias, P. C., (1997). "Determination of monotonic stress-strain curve of hard materials from ultra-low-load indentation tests", *International Journal of Solids and Structures*, 35: 365-381.
- [28] Huber, N., and Tsakmakis, C., (1999). "Determination of constitutive properties from spherical indentation data using neural networks. Part II: plasticity with nonlinear isotropic and kinematic hardening", *Journal of the Mechanics and Physics of Solids*, 47 (7): 1589-1607.
- [29] Giannakopoulos, A. E., and Suresh, S., (1999). "Determination of elastoplastic properties by instrumented sharp indentation", *Scripta Materialia*, 40: 1191–1198.
- [30] Tunvisut, K., Busso, E. P., O’Dowdy, N. P., and Brantner, H. P., (2002). "Determination of the mechanical properties of metallic thin films and substrates from indentation tests", *Philosophical Magazine A*, 82: 2013-2029.
- [31] Beghini, M., Bertini, L., and Fontanari, V., (2005). "Evaluation of the stress–strain curve of metallic materials by spherical indentation", *International Journal of Solids and Structures*, 43: 2441–2459.
- [32] Kim, J. Y., Lee, K. W., Lee, J. S., and Kwon, D., (2006). "Determination of tensile properties by instrumented indentation technique: Representative stress and strain approach", *Surface & Coatings Technology*, 201 (7): 4278-4283.
- [33] Tyulyukovskiy, E., and Huber, N., (2006). "Identification of viscoplastic material parameters from spherical indentation data: Part I. Neural networks", *Journal of Materials Research*, 21 (3): 664-676.
- [34] Klotzer, D., Ullner, C., Tyulyukovskiy, E., and Huber, N., (2006). "Identification of viscoplastic material parameters from spherical indentation data: Part II. Experimental validation of the method", *Journal of Materials Research*, 21 (3): 677-684.
- [35] Lau, K. T., Chipara, M., Ling, H. Y., and Hui, D., (2004). "On the effective elastic moduli of carbon nanotubes for nanocomposite structures", *Composites Part B-Engineering*, 35 (2): 95-101.
- [36] Yu, M. F., Lourie, O., Dyer, M. J., Moloni, K., Kelly, T. F., and Ruoff, R. S., (2000). "Strength and breaking mechanism of multiwalled carbon nanotubes under tensile load", *Science*, 287 (5453): 637-640.
- [37] Tjong, S. C., (2006). "Structural and mechanical properties of polymer nanocomposites", *Materials Science & Engineering R-Reports*, 53 (3-4): 73-197.
- [38] Strök, M., (2006). "'The structures of eight allotropes of carbon' under the GNU Free Documentation License", http://en.wikipedia.org/wiki/Allotropes_of_carbon: 08.04.2012.
- [39] Chang, T. C., Geng, J. Y., and Guo, X. M., (2005). "Chirality- and size-dependent elastic properties of single-walled carbon nanotubes", *Applied Physics Letters*, 87 (25).

- [40] Zaman, I., Phan, T. T., Kuan, H. C., Meng, Q. S., La, L. T. B., Luong, L., Youssf, O., and Ma, J., (2011). "Epoxy/graphene platelets nanocomposites with two levels of interface strength", *Polymer*, 52 (7): 1603-1611.
- [41] Zaeri, M. M., Ziaei-Rad, S., Vahedi, A., and Karimzadeh, F., (2010). "Mechanical modelling of carbon nanomaterials from nanotubes to buckypaper", *Carbon*, 48 (13): 3916-3930.
- [42] Kotov, N. A., (2006). "Materials science: Carbon sheet solutions", *Nature*, 442 (7100): 254-255.
- [43] Lee, C., Wei, X. D., Kysar, J. W., and Hone, J., (2008). "Measurement of the elastic properties and intrinsic strength of monolayer graphene", *Science*, 321 (5887): 385-388.
- [44] Ramanathan, T., Abdala, A. A., Stankovich, S., Dikin, D. A., Herrera-Alonso, M., Piner, R. D., Adamson, D. H., Schniepp, H. C., Chen, X., Ruoff, R. S., Nguyen, S. T., Aksay, I. A., Prud'homme, R. K., and Brinson, L. C., (2008). "Functionalized graphene sheets for polymer nanocomposites", *Nature Nanotechnology*, 3 (6): 327-331.
- [45] Sakhaee-Pour, A., (2009). "Elastic properties of single-layered graphene sheet", *Solid State Communications*, 149 (1-2): 91-95.
- [46] Zhu, J., Kim, J. D., Peng, H. Q., Margrave, J. L., Khabashesku, V. N., and Barrera, E. V., (2003). "Improving the dispersion and integration of single-walled carbon nanotubes in epoxy composites through functionalization", *Nano Letters*, 3 (8): 1107-1113.
- [47] Schniepp, H. C., Li, J. L., McAllister, M. J., Sai, H., Herrera-Alonso, M., Adamson, D. H., Prud'homme, R. K., Car, R., Saville, D. A., and Aksay, I. A., (2006). "Functionalized single graphene sheets derived from splitting graphite oxide", *Journal of Physical Chemistry B*, 110 (17): 8535-8539.
- [48] Potschke, P., Bhattacharyya, A. R., and Janke, A., (2003). "Morphology and electrical resistivity of melt mixed blends of polyethylene and carbon nanotube filled polycarbonate", *Polymer*, 44 (26): 8061-8069.
- [49] Das, B., Prasad, K. E., Ramamurty, U., and Rao, C. N. R., (2009). "Nano-indentation studies on polymer matrix composites reinforced by few-layer graphene", *Nanotechnology*, 20 (12).
- [50] Liang, J. J., Huang, Y., Zhang, L., Wang, Y., Ma, Y. F., Guo, T. Y., and Chen, Y. S., (2009). "Molecular-Level Dispersion of Graphene into Poly(vinyl alcohol) and Effective Reinforcement of their Nanocomposites", *Advanced Functional Materials*, 19 (14): 2297-2302.
- [51] Lau, K. T., Gu, C., and Hui, D., (2006). "A critical review on nanotube and nanotube/nanoclay related polymer composite materials", *Composites Part B-Engineering*, 37 (6): 425-436.
- [52] Li, D., Muller, M. B., Gilje, S., Kaner, R. B., and Wallace, G. G., (2008). "Processable aqueous dispersions of graphene nanosheets", *Nature Nanotechnology*, 3 (2): 101-105.

- [53] Eizenberg, M., and Blakely, J. M., (1979). "Carbon monolayer phase condensation on Ni(III)", *Surface Science*, 82: 228-236.
- [54] Berger, C., Song, Z. M., Li, X. B., Wu, X. S., Brown, N., Naud, C., Mayou, D., Li, T. B., Hass, J., Marchenkov, A. N., Conrad, E. H., First, P. N., and de Heer, W. A., (2006). "Electronic confinement and coherence in patterned epitaxial graphene", *Science*, 312 (5777): 1191-1196.
- [55] Hummers, W. S., and Offeman, R. E., (1958). "Preparation of graphitic oxide", *Journal of American Chemical Society*, 80: 1339.
- [56] Worsley, K. A., Ramesh, P., Mandal, S. K., Niyogi, S., Itkis, M. E., and Haddon, R. C., (2007). "Soluble graphene derived from graphite fluoride", *Chemical Physics Letters*, 445 (1-3): 51-56.
- [57] Niyogi, S., Bekyarova, E., Itkis, M. E., McWilliams, J. L., Hamon, M. A., and Haddon, R. C., (2006). "Solution properties of graphite and graphene", *J Am Chem Soc*, 128 (24): 7720-7721.
- [58] Paul, D. R., and Robeson, L. M., (2008). "Polymer nanotechnology: Nanocomposites", *Polymer*, 49 (15): 3187-3204.
- [59] Zeng, Q. H., Yu, A. B., Lu, G. Q., and Paul, D. R., (2005). "Clay-based polymer nanocomposites: Research and commercial development", *Journal of Nanoscience and Nanotechnology*, 5 (10): 1574-1592.
- [60] Goettler, L. A., Lee, K. Y., and Thakkar, H., (2007). "Layered silicate reinforced polymer nanocomposites: Development and applications", *Polymer Reviews*, 47 (2): 291-317.
- [61] Gao, L., Zhou, X. F., and Ding, Y. L., (2007). "Effective thermal and electrical conductivity of carbon nanotube composites", *Chemical Physics Letters*, 434 (4-6): 297-300.
- [62] Ma, J., Xu, H., Ren, J. H., Yu, Z. Z., and Mai, Y. W., (2003). "A new approach to polymer/montmorillonite nanocomposites", *Polymer*, 44 (16): 4619-4624.
- [63] Ma, J., Xiang, P., Mai, Y. W., and Zhang, L. Q., (2004). "A novel approach to high performance elastomer by using clay", *Macromolecular Rapid Communications*, 25 (19): 1692-1696.
- [64] Ma, J., Yu, Z. Z., Kuan, H. C., Dasari, A., and Mai, Y. W., (2005). "A new strategy to exfoliate silicone rubber/clay nanocomposites", *Macromolecular Rapid Communications*, 26 (10): 830-833.
- [65] Zandiatashbar, A., Picu, R. C., and Koratkar, N., (2012). "Mechanical Behavior of Epoxy-Graphene Platelets Nanocomposites", *ASME Journal of Engineering Materials and Technology*, In Press (
- [66] Rafiee, M. A., Rafiee, J., Srivastava, I., Wang, Z., Song, H. H., Yu, Z. Z., and Koratkar, N., (2010). "Fracture and Fatigue in Graphene Nanocomposites", *Small*, 6 (2): 179-183.
- [67] O'Neill, H. (1934). *The Hardness of Metals and Its Measurement* Chapman and Hall, Ltd., London.

- [68] Bowden, F. P., and Tabor, D., (1939). "The area of contact between stationary and between moving surfaces", *Proceedings of the Royal Society-A*, 169: 391.
- [69] Hutchings, I. M., (2009). "The contributions of David Tabor to the science of indentation hardness", *Journal of Materials Research*, 24 (3): 581-589.
- [70] Tabor, D., (1951). "The hardness and strength of metals", *Journal of the Institute of Metals*, 79 (
- [71] Newey, D., Wilkins, M. A., and Pollock, H. M., (1982). "An Ultra-Low-Load Penetration Hardness Tester", *Journal of Physics E-Scientific Instruments*, 15 (1): 119-122.
- [72] Loubet, J. L., Georges, J. M., Marchesini, O., and Meille, G., (1984). "Vickers Indentation Curves of Magnesium-Oxide (Mgo)", *Journal of Tribology-Transactions of the Asme*, 106 (1): 43-48.
- [73] Wierenga, P. E., and Franken, A. J. J., (1984). "Ultramicroindentation Apparatus for the Mechanical Characterization of Thin-Films", *Journal of Applied Physics*, 55 (12): 4244-4247.
- [74] tabor, D., and Stilwell, N. A., (1961). "Elastic recovery of conical indentations", *Proceedings of Physical Society*, 78: 169.
- [75] Berkovich, E. S., (1950). "Three-Faceted Diamond Pyramid for Studying Microhardness by Indentation", 13: 345-347.
- [76] Sneddon, I. N., (1948). "Boussinesq's problem for a rigid cone", *Proceeding of Cambridge Philosophy of Society*: 492-507.
- [77] Boussinesq, J., (1885). "Applications des Potentials a l'Etude de l'Equilibre et du Mouvement des Solides Elastiques", (
- [78] Cheng, Y. T., and Cheng, C. M., (1998). "Scaling approach to conical indentation in elastic-plastic solids with work hardening", *Journal of Applied Physics*, 84 (3): 1284-1291.
- [79] Cheng, Y. T., and Cheng, C. M., (2004). "Scaling, dimensional analysis, and indentation measurements", *Materials Science & Engineering R-Reports*, 44 (4-5): 91-149.
- [80] Knapp, J. A., Follstaedt, D. M., Myers, S. M., Barbour, J. C., and Friedmann, T. A., (1999). "Finite-element modeling of nanoindentation", *Journal of Applied Physics*, 85 (3): 1460-1474.
- [81] Li, M., Chen, W. M., Liang, N. G., and Wang, L. D., (2004). "A numerical study of indentation using indenters of different geometry", *Journal of Materials Research*, 19 (1): 73-78.
- [82] Sakharova, N. A., Fernandes, J., Antunes, J. M., and Oliveira, M. C., (2009). "Comparison between Berkovich, Vickers and conical indentation tests: A three-dimensional numerical simulation study", *International Journal of Solids and Structures*, 46 (5): 1095-1104.
- [83] Khan, M. K., Hainsworth, S. V., Fitzpatrick, M. E., and Edwards, L., (2010). "A combined experimental and finite element approach for determining

mechanical properties of aluminium alloys by nanoindentation", *Computational Materials Science*, 49 (4): 751-760.

- [84] Huber, N., and Tsakmakis, C., (1999). "Determination of constitutive properties from spherical indentation data using neural networks. Part I: the case of pure kinematic hardening in plasticity laws", *Journal of the Mechanics and Physics of Solids*, 47 (7): 1569-1588.
- [85] Gamonpilas, C., and Busso, E. P., (2004). "On the effect of substrate properties on the indentation behaviour of coated systems", *Materials Science and Engineering a-Structural Materials Properties Microstructure and Processing*, 380 (1-2): 52-61.
- [86] Colak, O. U., and Zandiatashbar, A., (2012). "Fabrication of Graphene Platelet (GPL)-Epoxy Nanocomposites and Characterization by Nanoindentation", *Advanced Materials Research*, 445: 809-814.
- [87] Zandiatashbar, A., Picu, C. R., and Koratkar, N., (2011). "Depth sensing indentation of nanoscale graphene platelets in nanocomposite thin films", *Materials Research Society Symposium Proceedings*: 1-6.
- [88] Zhou, Y. X., Akanda, S. R., Jeelani, S., and Lacy, T. E., (2007). "Nonlinear constitutive equation for vapor-grown carbon nanofiber-reinforced SC-15 epoxy at different strain rate", *Materials Science and Engineering a-Structural Materials Properties Microstructure and Processing*, 465 (1-2): 238-246.
- [89] Avril, S., Pierron, F., Sutton, M. A., and Yan, J. H., (2008). "Identification of elasto-visco-plastic parameters and characterization of Luders behavior using digital image correlation and the virtual fields method", *Mechanics of Materials*, 40 (9): 729-742.
- [90] Miller, S. G., Bauer, J. L., Maryanski, M. J., Heimann, P. J., Barlow, J. P., Gosau, J. M., and Allred, R. E., (2010). "Characterization of epoxy functionalized graphite nanoparticles and the physical properties of epoxy matrix nanocomposites", *Composites Science and Technology*, 70 (7): 1120-1125.
- [91] Lemaitre, J., and Chaboche, J. L. *Mechanics of Solid Materials*.
- [92] Xu, Z. H., and Li, X. D., (2008). "Effects of indenter geometry and material properties on the correction factor of Sneddon's relationship for nanoindentation of elastic and elastic-plastic materials", *Acta Materialia*, 56 (6): 1399-1405.

CURRICULUM VITAE

PERSONAL INFORMATION

Name Surname : Osman BAYRAK
Birth Date and Place : 17.11.1987, Bursa
Foreign Language : English
E-mail : osman.bayrak@hotmail.com.tr

EDUCATION

Degree	Subject	College/University	Graduation Year
B.Sc.	Mechanical Eng.	Selçuk University	2009
High School	Science	Emirsultan High School	2004

WORK EXPERIENCE

Year	Institution	Occupation
2012-	Bursa Technical University	Research Assistant
2010-2012	Yıldız Technical University	Research Assistant

Conference Paper

1. Nanoindentation and Finite Element Analysis of Graphene Platelet-Epoxy Nanocomposite 14th International Materials Symposium (IMSP'2012)